Design of a Magnetically Tunable Low Noise Amplifier in 0.13μm CMOS Technology

By

Jeremy L. Brown

A thesis submitted to the graduate faculty

in partial fulfillment of the requirements for the degree of

MASTER OF SCIENCE

Major: Electrical Engineering

Program of Study Committee:

Nathan Neihart, Major Professor
Degang Chen
Mani Mina

Iowa State University

Ames, Iowa

2012

TABLE OF CONTENTS

LIST OF FIGURES

ACKNOWLEDGEMENTS

I would like to thank Dr. Nathan M. Neihart for his financial support and all the help he has given me during my graduate studies at Iowa State University.

I would also like to thank my parents who supported me financially and emotionally throughout college and graduate school.

ABSTRACT

With legacy technologies present and approaching new wireless standards, the 1–10 GHz band of frequencies is quickly becoming saturated. Although saturated, the frequency bands are being utilized inefficiently. Cognitive radio, an intelligent wireless communication system, is the novel solution for the efficient utilization of the frequency bands. Front-end receivers for cognitive radio will need the capability to receive and process multiple frequency bands and a key component is the low noise amplifier (LNA). A tunable LNA using a new magnetically tuned input impedance matching network is presented. The LNA has been designed and simulated in a commercially available 0.13μm CMOS technology and is capable of tuning from 3.2 GHz to 4.6 GHz as S_{11} < -10 dB. Within this bandwidth the maximum power gain is 16.2 dB, the maximum noise figure is 7.5 dB, and the minimum IIP3 is -6.4 dBm. The total power consumption of the LNA (neglecting the buffer required to drive the 50 Ω test equipment) is 50 mW.

This tunable LNA introduces a new magnetically tunable matching technique and tuning scheme capable of continuous frequency variation for LNAs. It is expected that this technique could be expanded to realize LNAs with a tunable, narrow-band response that can cover the entire 1–10 GHz band of frequencies. The presented tunable LNA has demonstrated the capability to cover and process multiple frequencies and can be used for reconfigurable systems. A tunable LNA design is the first step in an effort to realize a fully reconfigurable front-end radio frequency (RF) receiver for future cognitive radio applications.

CHAPTER 1. INTRODUCTION

Radio transmitters are constrained to operate within a band of frequencies that has been set aside for their sole use by regulatory bodies. But with many legacy technologies present, and new wireless standards approaching, spectrum in the 1–10 GHz band of frequencies is quickly becoming saturated. Fig. 1 depicts the United States frequency allocations for 2011 [1], where each division is a licensed band reserved/brought for specific purposes. Even though the spectrum is saturated, many frequency bands are not always in use by the primary users, therefore wasting the unoccupied frequency prohibited from other users. Researchers are currently looking for ways to efficiently allocate the radio frequency spectrum for all users. This realization has led to the idea of a dynamic spectrum sensing, or "cognitive" radio.

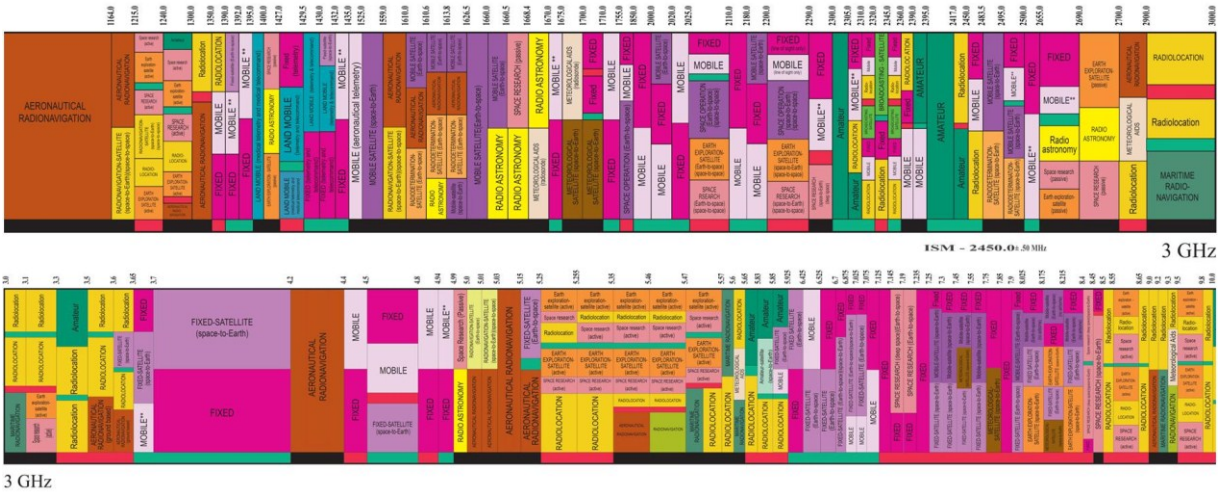

Fig. 1. U.S. 2011 frequency allocations.

The electromagnetic radio spectrum is a natural resource that includes all possible frequencies of electromagnetic radiation. Heavily utilized by transmitters and receivers, the radio spectrum is licensed and managed by governments. As earlier mentioned, the radio spectrum currently is used inefficiently with some bands unoccupied, others partially occupied and the remaining heavily used. Thus an approach is needed to improve the utilization of the radio spectrum. Cognitive radio (CR) is viewed as a novel approach for improving the utilization of the radio electromagnetic spectrum, a precious natural resource [2]. Defined as an intelligent wireless communication system, CR is aware of its surrounding environment and is capable of adapting to environmental changes by modifying certain operating parameters such as the transmit power, carrier frequency, or signal bandwidth, thus reconfigurable. CR is also capable to perform spectrum sensing, searching and detecting unoccupied frequencies, while communicating simultaneously [2].

In the last decade, cognitive radio has been the motivation for a vast amount of research in both the software and circuit design areas. Present CRs are focused toward the lower frequencies of the radio spectrum, such as TV bands [3]. However, with its properties, CRs will be targeting higher frequencies, such as the 1 – 10 GHz [4]. With the many advantages that CR possesses, there are some challenges present in their design. CR is expected to operate at any frequency in its range which requires synthesizers to provide a wide range of carrier frequencies and must tolerate interferers within the range [4].

Front-end receivers for cognitive radio will need the capability to receive and process multiple frequency bands. A basic front-end radio frequency (RF) receiver architecture is shown in Fig. 2.

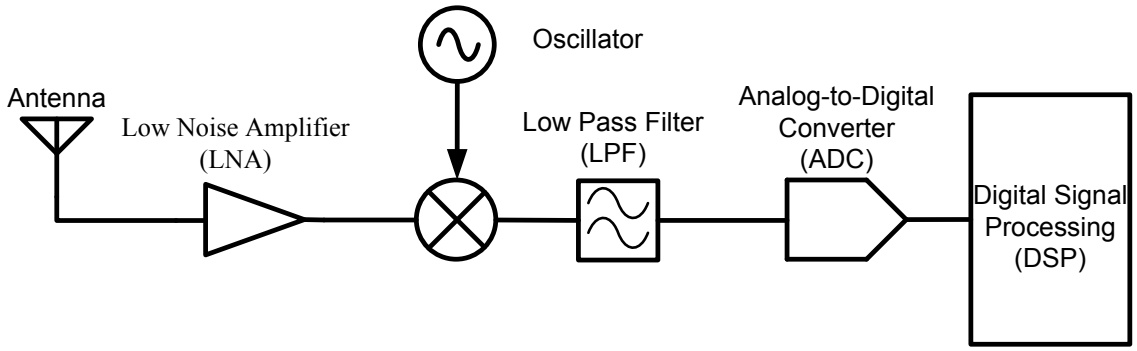

Fig. 2. Basic front-end radio frequency (RF) architecture.

For the front-end receiver to be reconfigurable, each component must also be reconfigurable and one key component is the low noise amplifier (LNA). A LNA is typically the first component used in the RF receiver chain. The LNA amplifies weak signals captured by the antenna while introducing minimum amounts of noise, as the name implies. The LNA is typically a narrowband component designed to receive and amplify a single frequency. For CRs, LNAs will need to have a broadband frequency response to operate at multiple frequencies, while maintaining its low noise figure, high gain and good linearity.

This work explores the use of impedance matching networks to achieve the broadband frequency response and introduces a new LNA design suitable for CRs. The remainder of this thesis is organized as follows: Chapter 2 reviews the current state-of-the-art in the field of ultra-wideband LNA design, Chapter 3 reviews the figure of merits associated with LNA design and how they trade-off with one another, the circuit level design and simulation results are presented in Chapter 4, and in Chapter 5, future work and applications are discussed.

CHAPTER 2. LITERATURE REVIEW

Cognitive radio is the novel approach for improving the utilization of the radio electromagnetic spectrum [2]. An intelligent wireless communication system that is aware of its environment, a cognitive radio has the ability to modify its receivers' and transmitters' operation parameters, such as transmit power, carrier frequency, and signal bandwidth. With these capabilities, cognitive radios will be able to provide efficient utilization of the radio spectrum. Front-end receivers for cognitive radio will need the capability to receive and process multiple frequency bands and one key component is the low noise amplifier (LNA). Traditionally, there are three approaches to realizing LNAs capable of receiving multiple frequency bands: wideband LNAs, multi-band LNAs, and tunable LNAs. Each of these classes will be discussed in greater detail in the following sections.

2.1 Wideband LNAs

The traditional LNA naturally has a narrowband input impedance matching network designed to receive a singular frequency. Wideband LNAs, on the other hand, have the capability to cover all of the desired frequency bands simultaneously via its wideband input impedance matching network. Generating a wideband network from a narrowband network is a challenging design issue, involving specific design combinations of passive and active elements. However, the need to receive multiple bands is significant for the realization of cognitive radio systems. Numerous wideband input matching techniques have been introduced and include the use of *LC* bandpass filtering, reactive feedback, resistive/source-follower feedback, and common-gate input stages.

2.1.1 LC Bandpass Filtering

The first technique for wideband input matching is the *LC* bandpass filtering, which typical achieves a bandwidth of 5 -7 GHz. This technique, which utilizes an inductor *L* and a capacitor *C* to form multiple bandpass filters, is placed at the input of the LNA. A bandpass filter is an electronic circuit that passes all the frequencies within a given bandwidth and rejects all other frequencies. Bandpass filters are created by the combination of low-pass and high-pass filters, therefore, increasing the range of accepted frequencies around center frequency. The low-pass and high-filter cutoff frequencies are placed at the high and low bounds of the desired bandwidth, respectively, thus creating a bandpass filter. The schematic of a LNA using a *LC* bandpass filter input impedance matching network [5] is shown in Fig. 3.

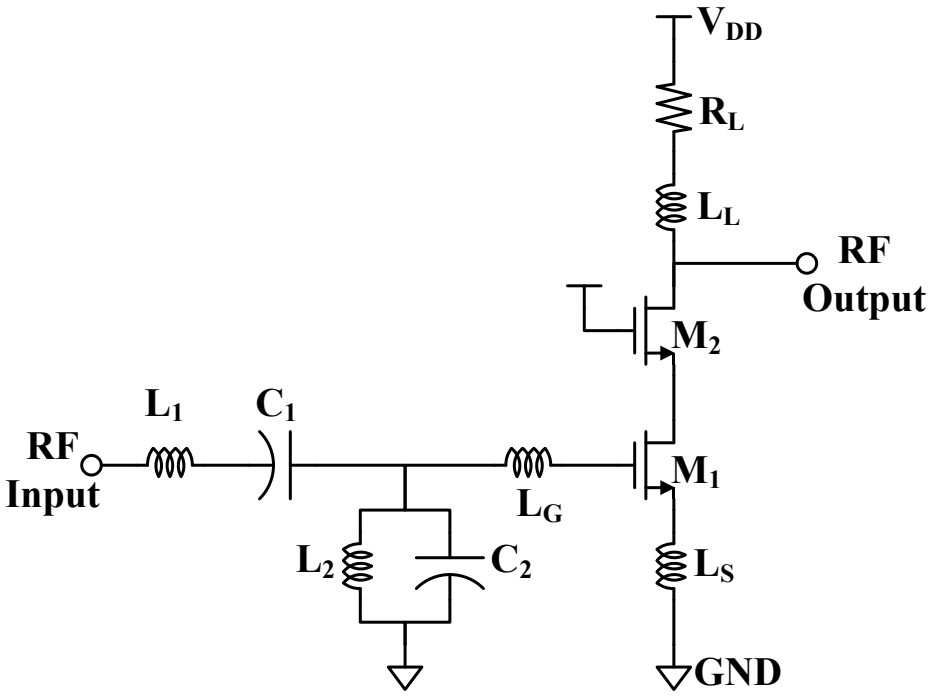

Fig. 3. Simplified schematic of a *LC* bandpass filter LNA.

The cascode configuration, M_1 and M_2, improves the input-output isolation and the amplifier's frequency response. The output network uses inductive peaking to extend the bandwidth of the output impedance. The buffer is intended to drive a 50 Ω load, for measurement purposes only. The wideband input matching network is comprised of the common-source amplifier's input network embedded into a multisection reactive network, a common three-section passband filter structure. The systems in [6] and [7] use a fourth-order *LC*-ladder bandpass filter and a third-order *LC* low-pass filter, respectively, for wideband impedance match. The system in [6] achieves a 7 GHz bandwidth, with high gain and low noise, but has high power consumption and large area is required, due to large bias current and four on-chip inductors respectively. The system in [7], on the contrary, achieves a bandwidth of 4.3 GHz with low gain and high noise. Due to one less inductor, [7] consumes smaller area than [6] but also requires large amount of power.

The system in [8] uses a transformer-based filter to achieve its wideband impedance match. The system utilizes a symmetric transformer, with the embedded common-source impedance, to obtain the bandpass filter for the impedance matching and to reduce area. The system [8] has high gain, acceptable noise, low power consumption and small area, due to the symmetric transformer. However, the system only has a 2 GHz bandwidth. The *LC* bandpass filter structure, regardless of order and/or type, resonates the overall reactance of the input matching network across the desired bandwidth. This technique typically achieves a wideband frequency response, high gain and moderate noise figure, based on design optimization. However, it has high power consumption and requires large area, due to the use of multiple inductors and capacitors.

2.1.2 Reactive Feedback

Reactive feedback is the second technique used to accomplish a wideband input match network, which generally attains greater than 6 GHz of bandwidth. Feedback is the process in which information from a system's output is returned to influence a system's input. Feedback is mainly used to control or maintain a system's performance. Fig. 4 shows the schematic of a reactive feedback LNA [9]. The circuit consists of a transformer L_G and L_D, and a transistor pair M_1 and M_2, which enhances the transconductance of the circuit. Two feedback paths are present, series inductive feedback via transformer and shunt capacitive feedback via parasitic gate-drain capacitance C_{GD}. The wideband matching is achieved by separating the desired bandwidth into low and high frequencies. Impedance matching at lower frequencies is achieved by the shunt capacitive feedback, higher frequencies by the series inductive feedback of the transformer.

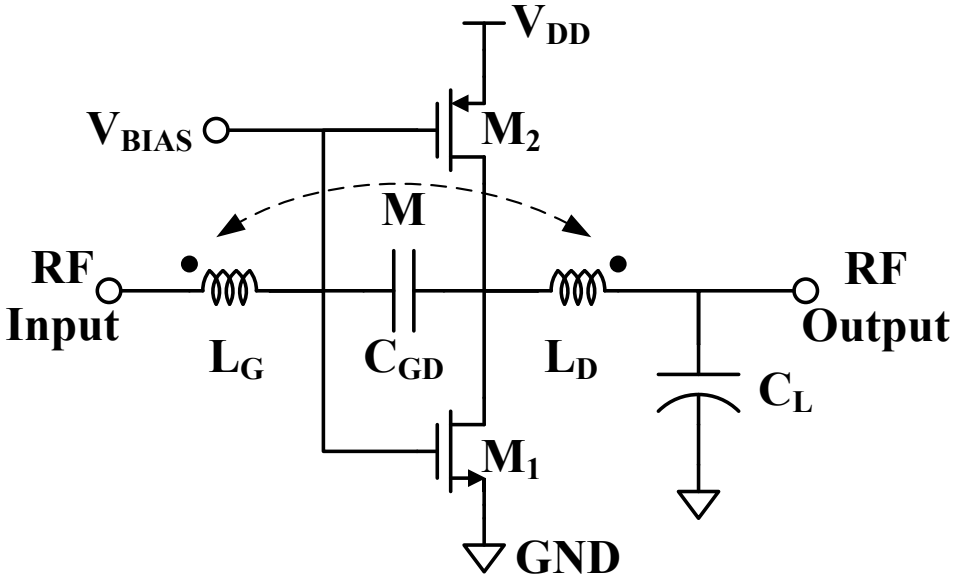

Fig. 4. Schematic of reactive feedback LNA.

This system's advantages are low power consumption and a 7 GHz bandwidth. Disadvantages are low gain, high noise and area consumption. The system in [10] uses a transformer to attain wideband impedance matching via magnetic coupling of the drain and gate currents of the input common-source amplifier, providing negative reactive feedback. The system has low power consumption, high gain, low noise and a 6 GHz bandwidth. Although the system was not fabricated, required area is still large due to usage of multiple inductors. The system in [11] also uses negative reactive feedback to accomplish wideband input impedance, via two implemented transformers for gain stabilization, reduced noise, and terminal impedance matching. The benefits of this system are high gain, low noise, low power consumption, and a 7 GHz bandwidth. The expense is the large required area for the two implemented inductors. This technique achieves low power consumption, and a wide frequency bandwidth. General drawbacks are high noise figure, low gain, and area consumption via transformers.

2.1.3 Resistive/Source Follower Feedback

The third technique for wideband input matching network is the resistive or source-follower feedback, capable of providing bandwidths wider than 6 GHz. In this technique, a resistor or a transistor is the source for feedback, instead of inductors. Fig. 5 shows the schematic of a LNA using the resistive feedback technique [12]. It basically consists of a common-source amplifier, cascode configuration, and an inductive load. Wideband input match is achieved by the shunt-shunt resistive feedback R_F in conjunction with the embedded common-source matching network. The system in [12] achieves low noise and a bandwidth of 27 GHz.

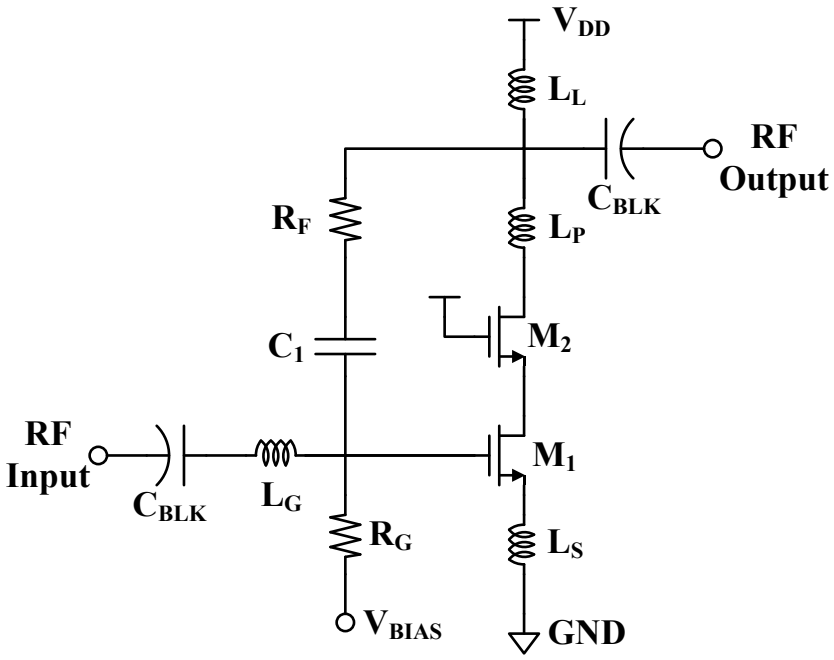

Fig. 5. Schematic of a resistive feedback LNA.

The drawbacks are low flat gain, high power consumption and large area, due to the use of four inductors. The systems in [13]-[15] combat the area consumption by eliminating the inductors. Inductorless systems use resistive and/or source follower feedback to set the wideband input impedance and optimize for area via load resistors. The system in [13] uses both techniques to achieve wideband match for 7 GHz, low noise, high gain and small area consumption. However, the system requires large amounts of power consumption. Other systems [16]-[18] utilize this technique will still incorporate inductors for gain peaking, low noise and small power consumption advantages. The system in [17] incorporates inductors and achieves low noise and small power consumption. Still, the system's shortcomings are low gain, large area consumption, and a 2 GHz bandwidth. Nonetheless, this technique requires extra circuitry, at least a resistor and/or source follower transistor configuration, to achieve good performance in noise and impedance match.

2.1.4 Common Gate Input Stage

A wideband input matching network can be design without adding any passive or feedback elements to the input signal path. A common gate input stage, a well-recognized technique [19]-[25], can achieve wideband input impedance itself, providing bandwidths over 6 GHz. A common-gate input stage LNA is shown in Fig. 6 [21]. It consists of a single transistor M_1, inductor L_1, and the transformer between L_L and L_S. Inductor L_1 extends the gain bandwidth and the input bandwidth. The transformer improves the noise figure by partial canceling the noise attributed to M_1 [21]. The wideband input impedance is achieved via the transconductance of M_1. The input impedance of a common-gate transistor, excluding any parasitics, is $1/g_{m1}$.

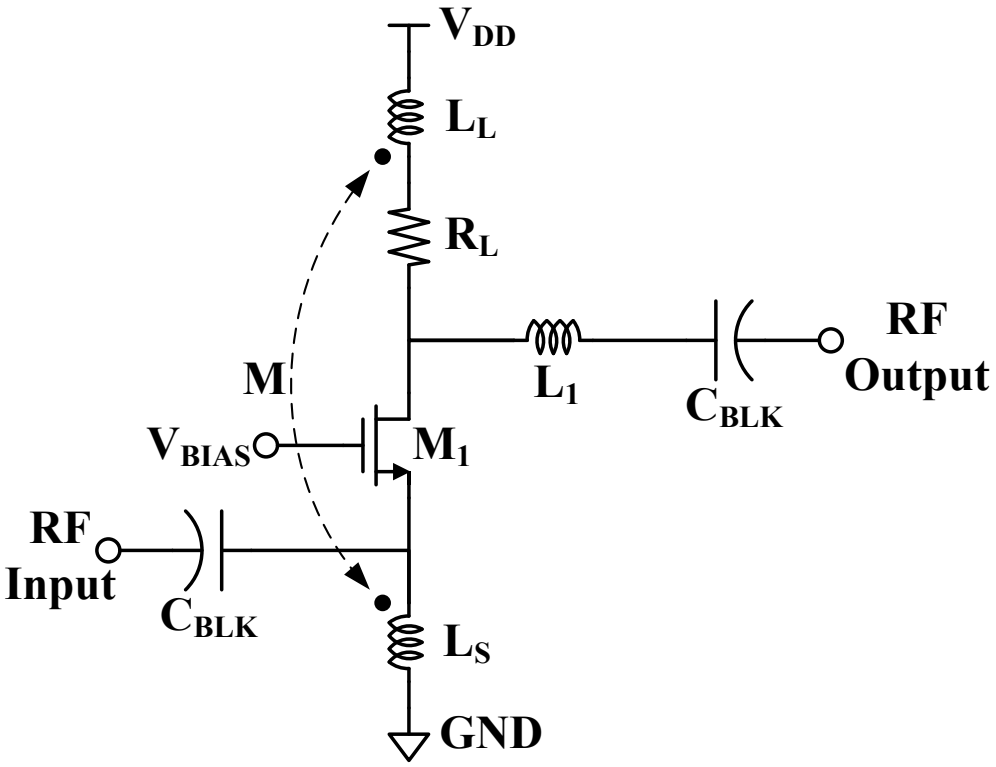

Fig. 6. Schematic of a common gate input LNA.

The input impedance is purely real and frequency independent, thus presenting wideband impedance at the input for 7 GHz bandwidth. Low power consumption, low noise, and reasonable area are some advantages of this system. The system in [21] has low gain without the use of the previously mentioned cascode configuration. The systems in [23] and [24] use the cascode configuration to overcome low gain of the single transistor common gate system. The system in [25] also uses cascode configuration for high gain and uses the *LC* bandpass filter technique previously mentioned only to achieve the same bandwidth as [21]. This system uses the *LC* bandpass filter to make its input matching network more robust against PVT (Process, Voltage and Temperature) variations [25], thus increasing the required area due to added passive components.

Noise cancellation is a mechanism which makes the common-gate input stage more attractive than other wideband amplifiers and there are many approaches that accomplish this goal. The transformer mechanism [21] forms a transformer via magnetic coupling of the input and output shunt peaking inductors. The noise sources generated at the input, via the common-gate transistor and signal noise, are negatively coupled through the transformer presenting scaled anti-phase and correlated noise sources at the output. At the output, the noise sources are added and thus partially cancelled reducing the noise figure of the LNA. The differential LNA is another noise cancellation mechanism [19], [24]. This mechanism uses a second stage common-source LNA, tied at the input of the common-gate LNA, to negatively amplify the noise sources present at the input for cancellation at the output. The noise source generated by the common-gate input stage induces an in-phase amplified noise

source at the output of the common-source LNA, thus the sources are nulled at the output via differential sensing [24].

The primary shortcomings for wideband LNAs is having a wideband frequency response can be problematic as it allows undesired interferers and noise across the bandwidth to pass through the LNA, placing stringent linearity requirements on the mixer and subsequent RF stages and higher noise figure. This is especially true in cognitive radio applications where a narrowband signal must be received and can be located anywhere within a large range of frequency. Multi-band and tunable LNAs can be used to combat this problem and thereby relax the linearity.

2.2 Multi-band LNAs

Multi-band LNAs are capable of receiving and processing multiple, narrowband signals across different wireless standards, as desired for cognitive radio. To receive multiple standards, the input and/or output impedance matching networks must be reconfigurable. Several multi-band techniques have been presented and include parallel, switching, and concurrent dual-band.

2.2.1 Parallel LNAs

Parallel LNAs are the easiest and simplest technique for multi-band LNAs. The parallel configuration involves taking multiple single frequency LNAs and placing them in parallel, tying the input and output ports together, respectively. A general block diagram of a parallel multi-band LNA scheme is shown in Fig. 7. The parallel LNA in Fig. 7 uses *M* LNAs to cover multiple wireless standards for RF receivers. The systems in [26]-[29] use at most three LNAs to receive the bands of interest.

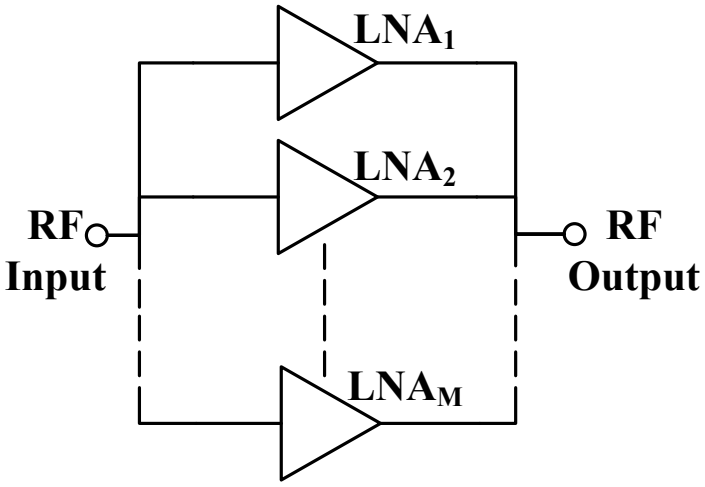

Fig. 7. Block diagram of parallel multi-band LNA.

Impedance matching, noise figure and gain are impeccable for this technique, due to each LNA being specifically designed for each specific frequency. However, the primary drawbacks of this technique are power and area consumption due to having multiple LNAs, each with multiple inductors within the design.

2.2.2 Switching LNAs

The most common technique for multi-band LNAs is the usage of switches, due to its simplicity and ease of implementation. Many switching multi-band LNAs implement tuning at the output of the amplifier, in order to avoid degrading the noise figure of the amplifier. While at the input, the LNAs maintain the wideband impedance matching. However, there are designs where switches are used at the input also [30]. A switching multi-band LNA is shown in Fig. 8 [31]. It consists of an inductive degenerative common-source amplifier, cascode configuration, and uses the resistive feedback technique previously mentioned. This design [31] uses a series of switched inductors in order to reconfigure the frequency response of the output network only able to cover three specific frequencies, 900 MHz,

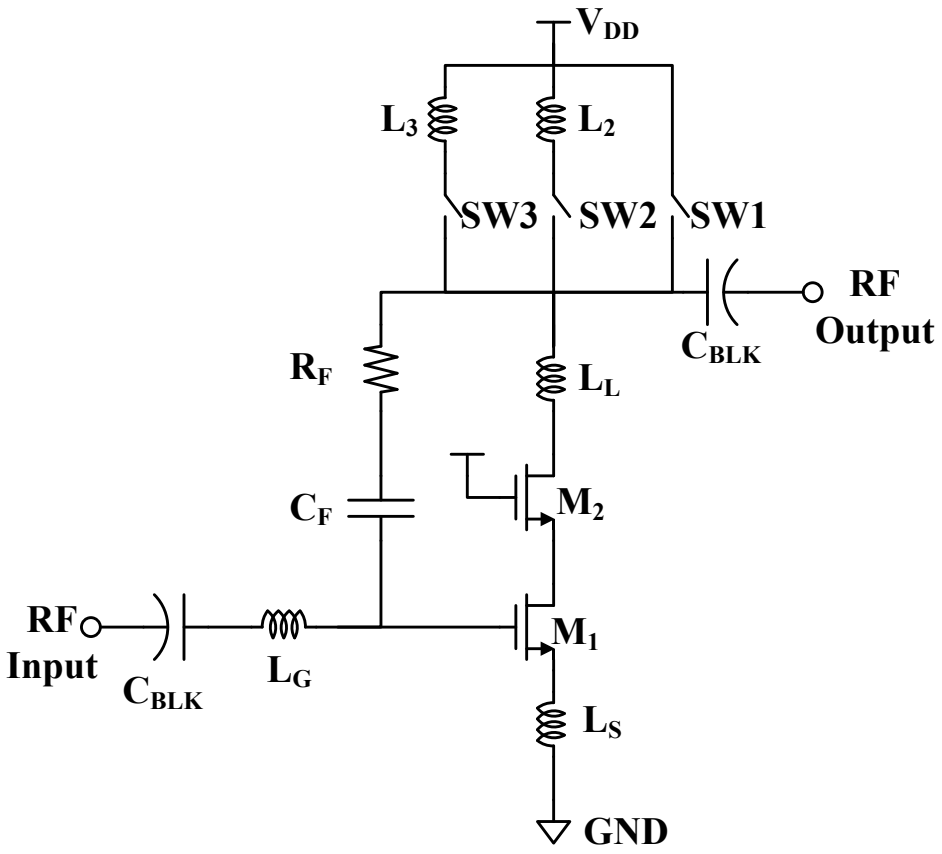

Fig. 8. A switching multi-band LNA.

1.8 GHz and 5.2 GHz. The primary drawback of this system is the need for multiple inductors in the load, which increases the required area.

The systems in [32] and [33] get around this problem by using a tapped inductor and a transformer, respectively. While the tapped inductor reduces the extra area required by the load, the system in [32] still utilizes an LC bandpass filter to achieve a wideband input impedance match and thus is still quite area intensive. The system in [33], on the other hand, requires only a single inductor in the input of the LNA and thereby reduces the overall area. The primary drawback for switching LNAs is that bands of interest are not received simultaneously and are not continuous. Other drawbacks are the use of switches degrades the

quality factor of inductors, thus the output frequency response becomes broadband, and decreases the gain of the LNA.

2.2.3 Concurrent Dual-Band LNAs

Concurrent LNAs, as opposed to switching, can receive all interested bands simultaneously without the use of switches to reconfigure its frequency response of matching networks. For the concurrent technique, both input and output matching networks must be designed to have identical operating frequencies for the LNA to properly receive the signals. A concurrent multi-band LNA [34] is shown in Fig. 9.

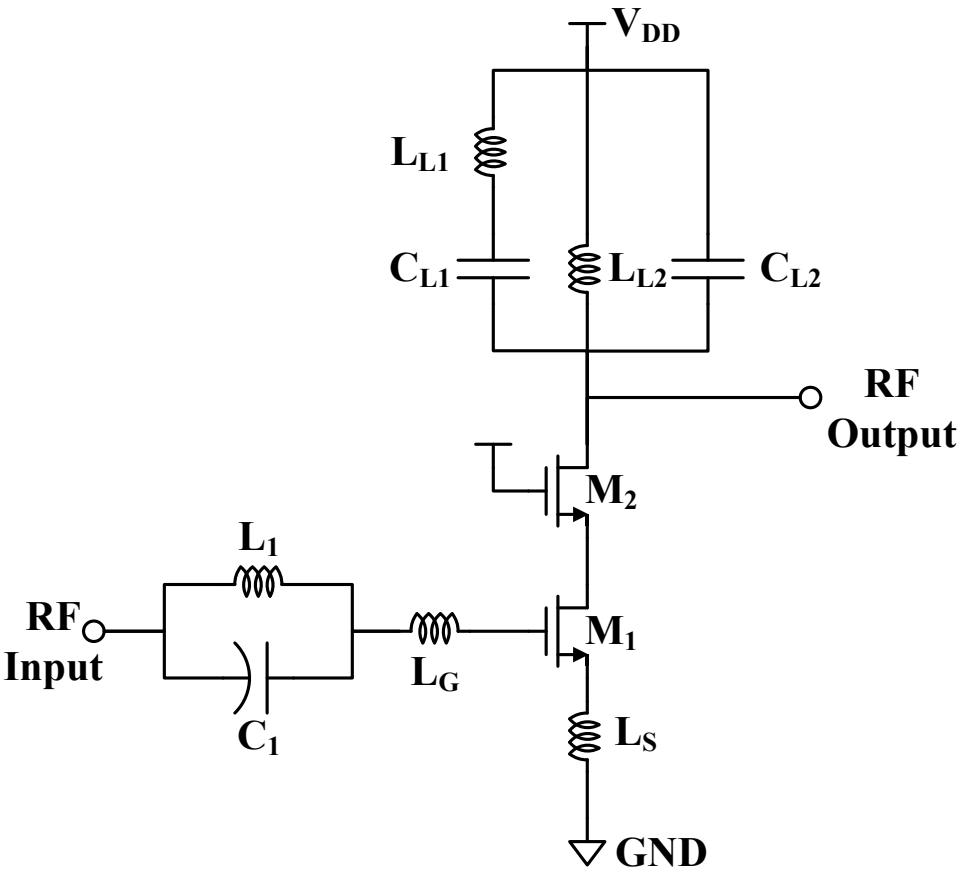

Fig. 9. Schematic of a concurrent multi-band LNA.

The system consists of an inductive degenerative common-source amplifier and a cascode configuration for good reverse isolation of the input and output ports. The concurrent technique uses a series resonant *LC* and two *LC* resonant tanks for the input and output matching networks, respectively. These matching networks are narrowband and designed for the desired frequencies, unlike wideband LNAs. The systems in [35] and [36] also share the same architecture shown in Fig. 9. This technique achieves great noise figure, impedance matching, and moderate gain at the design frequencies. The drawbacks for this technique and design are large required area, due to multiple inductors, and lack of flexibility, as they cannot change from their designed frequencies.

Overall, the major weakness of multi-band LNAs is that they are not continuously tunable over the radio frequency spectrum and therefore unsuitable for applications such as cognitive radio. Tunable LNAs can be used to resolve this problem.

2.3 Tunable LNAs

Tunable LNAs can provide continuous frequency variation across a desired frequency range. A combination of wideband and multi-band, tunable LNAs have both wide frequency bandwidths with the selectivity of all frequencies within the given range. There are two methods for achieving frequency tuning, reconfigurable matching networks at the input and/or output.

2.3.1 Output Tuning LNAs

Frequency tuning at the output is defined by the capability to reconfigure the frequency response of the output impedance, generally attaining bandwidths of 4 GHz. Several techniques for output frequency tuning have been presented and include tunable *LC* tank via

variable capacitance and variable inductance. Variable capacitance is method of varying the capacitance of the load *LC* tank, usually achieved via a varactor diode or a varactor MOSFET configuration. A tunable LNA using the variable capacitance technique is shown in Fig. 10 [37].

The system uses an inductively degenerated cascode common-source amplifier configuration with inductive peaking load. The system uses a three section bandpass filter structure to achieve wideband input impedance matching over the desired frequencies, like previously mentioned systems [6]-[8]. Frequency tuning occurs at the output via the varactor C_{VAR}, which adds capacitance as the bias voltage V_{TUNE} increases, reconfiguring the narrowband frequency response of the output impedance. The bandwidth of output network is narrowband and as V_{TUNE} increase, the center frequency of the output impedance network

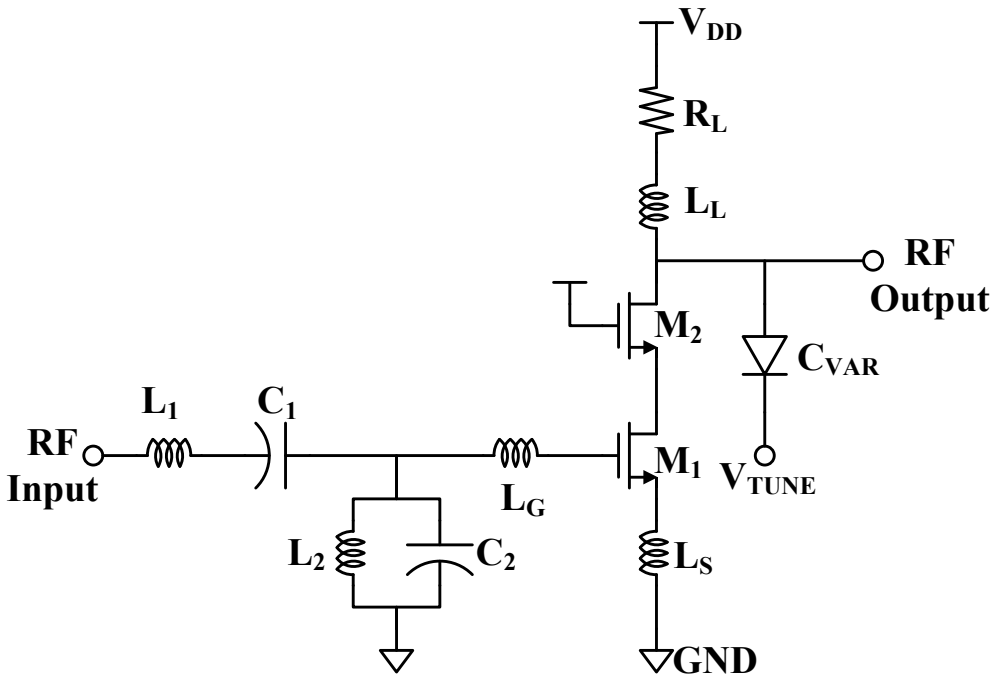

Fig. 10. Schematic of variable capacitor tunable LNA.

increases, thus having a tuning range of 4 GHz. This system has low power consumption, reasonable noise figure. The drawbacks of [37] are low gain and large area consumption. The system in [38] uses a varactor and switching inductors to extend its tuning range to 5 GHz, implementing both the variable capacitance and switching technique mentioned earlier. The system in [39] uses the variable inductor technique, altering the load inductance instead of the capacitance. The system places a metal or ferromagnetic plate above the inductor and by moving the position of the plate, the series inductance can be varied. These systems have high noise figures, acceptable gain and large area consumption. One shortcoming of output tunable LNAs is still the need for additional passive elements (including inductors) for the wideband input impedance matching, which dramatically increases the required area.

2.3.2 Input Tuning LNAs

Input tunable LNAs are relatively scarce compared to its counterpart. Frequency tuning at the input is defined by the capability to reconfigure the frequency response of the input impedance, which is inherently narrowband for common LNAs. The conventional LNA input is an inductive degenerative common-source amplifier with an inductor at its gate, shown in Fig. 11.

The input impedance matching of the amplifier is:

$$Z_{in} = \frac{g_{m1}L_S}{C_{gs1}} + j\left[\omega(L_S + L_G) - \frac{1}{\omega C_{gs1}}\right] \tag{2.1}$$

where g_{m1} is the transconductance of M_1, C_{gs1} is the parasitic gate-to-source capacitance of M_1, and ω_o is the resonant frequency of the input impedance network. The real part of the

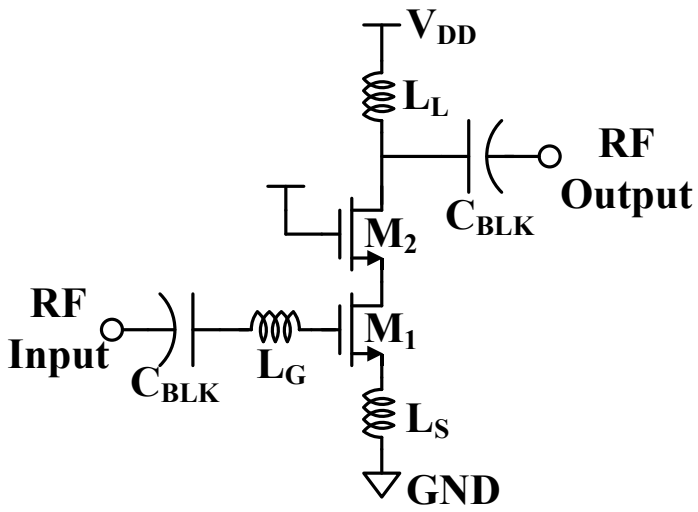

Fig. 11. Schematic of a conventional narrowband LNA.

impedance is frequency independent and the operation/resonant frequency is determined by L_G, L_S, and C_{gs1}.

From (2.1), there is only one component that does not affect both the real and imaginary parts of the input impedance, L_G. To achieve any reconfigurability of the input impedance, L_G must be variable. The switching technique via multiple inductors could possibly solve this issue, however, it comes with significant drawbacks as mentioned earlier. Another possible solution is the use of active inductors to replace passive inductors. An active inductor can be realized by connecting a MOSFET, in combination with capacitors and resistors, in such a way that the impedance looking into a terminal increases with frequency. The advantages of active inductors are its compact size and wide inductance value range. The disadvantage is the active inductor introduces noise into the system, thus increasing the LNA's noise figure. The proposed LNA system has applied a new technique which has the ability to vary the inductor L_G, thus achieving frequency tuning at the input of the LNA.

Tunable LNAs, via the narrowband input impedance, can provide continuously frequency variation, which inherently reject undesired signals and interferers, while adding minimum noise to the signal. Therefore, input tunable LNAs are suitable for many applications, including cognitive radio.

CHAPTER 3. TUNABLE LNA DESIGN

In the previous chapter, it can be concluded that tunable LNAs provide continuous frequency variation and achieve an impedance match that is reconfigurable for multi-standard, multi-band wireless systems. The drawbacks for tunable LNAs are large required area and higher noise figure. In this Chapter, the performance metrics of a conventional LNA will be examined, a new technique for input impedance match will be introduced, and then a new design will be proposed that address the shortcomings of tunable LNAs.

3.1 LNA Analysis

As with all systems, there are performance trade-offs and designs for specific applications. The performance parameters that define the merit of a LNA are input impedance, noise, linearity, and gain. To achieve a tunable LNA for desired applications, an analysis of a conventional narrow-band, inductively degenerated LNA, shown in Fig. 12, will be discussed.

3.1.1 Input Impedance

A very important parameter of the LNA is the input impedance, commonly set to 50 Ω. The quality of the input impedance matching network is measured by the scattering parameter S_{11}. Scattering parameters, or S-parameters, are used to characterize linear electronic networks [40]. The input port of an LNA is assigned port 1, therefore, S_{11} will be a complex number representing the ratio of how much power is reflected from port 1 to how much power is delivered to port 1. The magnitude of S_{11} expressed in units of decibels (dB) is desired to be very small ($S_{11} = -\infty$ for a perfect impedance match).

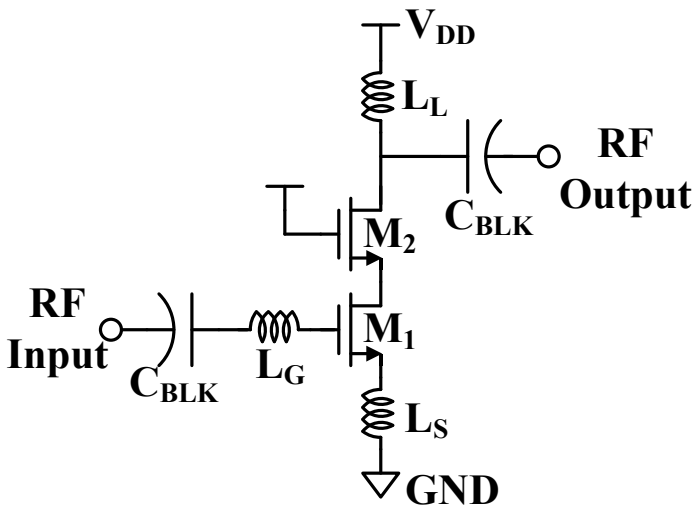

Fig. 12. Schematic of a conventional narrowband LNA.

The input impedance of this system in Fig. 12 can be expressed using the well-known equations:

$$Z_{in} = \frac{g_{m1}L_S}{C_{gs1}} + j\left[\omega(L_S + L_G) - \frac{1}{\omega C_{gs1}}\right] \tag{3.1}$$

where C_{gs1} and g_{m1} is the gate-to-source capacitance and transconductance of transistor M_1, respectively. The frequency at which the input impedance of the LNA is purely real is expressed as:

$$\omega_0 = \frac{1}{\sqrt{C_{gs1}(L_S+L_G)}}. \tag{3.2}$$

$$Real\{Z_{in}\} = \frac{g_{m1}L_S}{C_{gs1}} \tag{3.3}$$

It is seen from (3.2) and (3.3) that, while the operation frequency (i.e., the frequency at which Z_{in} is purely real) is determined by both L_S and L_G, the value of the real part of Z_{in} is

dependent upon L_S only. Therefore, by varying the value of L_G, the operation frequency of the LNA can be varied while maintaining a fixed, real-valued input impedance (e.g., 50 Ω).

3.1.2 Noise

Noise, a very important parameter, is anything outside of the desired signal. Noise performance of a radio frequency system is quantified by the noise factor *F*, a measure of how much noise the system adds to the signal being processed [41].

$$F = \frac{total\ output\ noise\ power}{output\ noise\ due\ to\ input\ source} \tag{3.3}$$

The noise figure , *NF*, is another measure of noise expressed in units of decibels (dB) and is defined as:

$$NF = 10\log_{10}(F) \tag{3.4}$$

Implied by its name, it is highly desirable that LNAs inject as little noise as possible while amplifying the signal. As the first component of the receiver, it is imperative that the system has low noise due to the following reasons. Consider the noise figure of a cascaded system shown in Fig. 13.

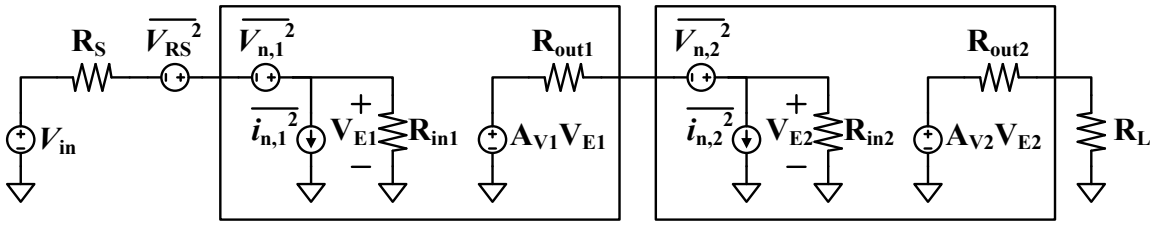

Fig. 13. Cascade of two noisy stages.

From Fig. 13, V_{in} is the input voltage source, R_S is the source resistance, and V_{RS} is the modeled source noise generator. V_n and i_n are the modeled voltage and current noise generators for each stage, respectively. R_{in} and R_{out} are the input and output resistances for each stage, respectively. R_L is the load resistor and A_V is the unloaded voltage gain of their respective stage.

The total noise figure of this two-stage system [3.2] can be derived as equation (3.5).

$$F_{tot} = 1 + \frac{\overline{|V_{n1} + i_{n1}R_S|^2}}{\overline{V_{RS}{}^2}} + \frac{\overline{|V_{n2} + i_{n2}R_{out1}|^2}}{\overline{V_{RS}{}^2}} \frac{1}{A_{V1}{}^2\left(\frac{R_{in1}}{R_S + R_{in1}}\right)^2} \tag{3.5}$$

Using the available power gain concept [42], (3.5) can be simplified and expressed in general terms of noise figure of different stages as (3.6). Available power gain is the power available at the output divided by the available power at the source. In the case of Fig. 13, the available output and available source powers of stage 1 are:

$$P_{out,av} = \frac{\left(A_{V1}V_{E1}/_2\right)^2}{2R_{out1}} = V_{in}^2\left(\frac{R_{in1}}{R_S + R_{in1}}\right)^2 A_{V1}^2 \frac{1}{8R_{out1}}, \tag{3.6}$$

$$P_{source,av} = \frac{\left(V_{in}/_2\right)^2}{2R_S} = \frac{V_{in}^2}{8R_S}. \tag{3.7}$$

Thus the available power gain G_{A1} of stage 1 is:

$$G_{A1} = \frac{P_{out,av}}{P_{source,av}} = A_{V1}{}^2\left(\frac{R_{in1}}{R_S + R_{in1}}\right)^2 \frac{R_S}{R_{out1}}. \tag{3.8}$$

Looking at the second term in of F_{tot} from (3.5), it can be seen that GA1 can be substituted in to define F_2 as:

$$F_2 = \frac{\overline{|V_{n2} + i_{n2}R_{out1}|^2}}{\overline{V_{RS}{}^2}} \frac{R_S/R_{out1}}{G_{A1}} \tag{3.9}$$

It is important to note the noise figure of stage 2 is with respect to the source impedance driving that stage [41]. Now the total noise figure in Fig. 13 can be expressed as:

$$F_{tot} = F_1 + \frac{F_2 - 1}{G_{A1}} \tag{3.10}$$

where $F_1 = 1 + \frac{\overline{|V_{n1} + i_{n1}R_S|^2}}{\overline{V_{RS}{}^2}}$ is the noise figure of stage 1 with respect to its source impedance R_S, F_2 is the noise figure of stage 2 with respect to its source impedance R_{out1}, and G_{A1} is the available power gain of stage 1. Similarly, if (3.10) is expanded to m stages, the equation becomes:

$$F_{tot} = F_1 + \frac{F_2 - 1}{G_{A1}} + \frac{F_3 - 1}{G_{A1}G_{A2}} + \cdots + \frac{F_m - 1}{G_{A1} \ldots G_{A(m-1)}} \tag{3.11}$$

This is known as Friis equation [42]. From (3.11), the noise figure of any given stage is reduced by the power gain of the preceding stages. The result is that the total receiver noise figure is dominated by the first few stages. Since the LNA is the first stage, the noise figure is added directly to the receiver system. This is the motivation why the LNA needs to have a low noise figure.

In LNA design, placing noisy components at the input is generally avoided so as to achieve the lowest possible noise figure. There are many noise sources in Fig. 12 that contributed to the noise figure of the LNA. For simplicity and clarity, only thermal noise is considered and all inductors and capacitors are considered to be ideal. The total short-circuit output noise current is comprised of effects from three primary noise sources: noise from the

source, $\overline{i_{n,s}^2}$, drain noise of M_1, $\overline{i_{n,d1}^2}$, and thermal noise from the load resistor R_L, $\overline{i_{n,rl}^2}$. It is assumed that M_2 does not significantly contribute to the total short-circuit output noise current. The short circuit output current for the conventional LNA noise figure shown in Fig. 14 is derived.

An expression for the output noise current due to the source can be written as:

$$i_{out,1} = \frac{g_{m1}R_S i_{n,s}}{s^2 C_{gs1}(L_G+L_S)+s(C_{gs1}R_S+g_{m1}L_S)+1}. \tag{3.12}$$

Next the driving transistor, M_1, is considered. As stated previously, only thermal drain current is considered in this analysis and the short-circuit output noise current due to M_1 can be expressed as:

$$i_{out,2} = i_{n,d1} - \frac{s g_{m1}L_S i_{n,d1}}{s^2 C_{gs1}(L_G+L_S)-s(C_{gs1}R_s-g_{m1}L_S)+1}. \tag{3.13}$$

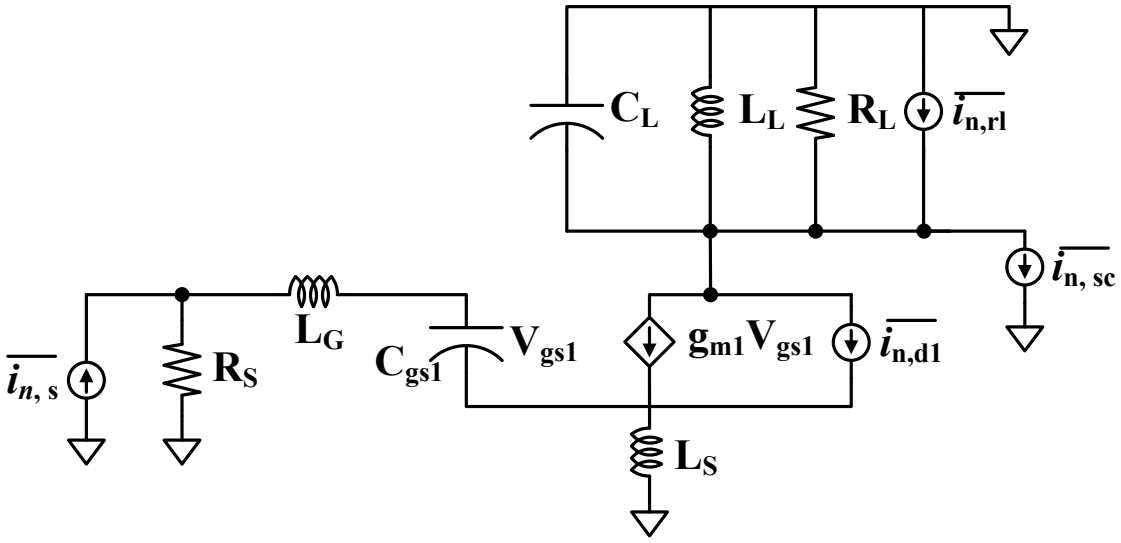

Fig. 14. Conventional LNA noise sources.

From (3.13), it is seen that part of the drain noise is by the input matching network and the other part is directly added to the total output noise current. For the conventional LNA, the drain noise of M_1 is a main contributor to the overall noise figure [43]. Finally the load resistor, R_L, is considered. The short-circuit output noise current due to R_L can be expressed as:

$$i_{out,3} = i_{n,rl}. \tag{3.14}$$

The total mean-squared noise current at the output of the LNA is simply the superposition of the individual mean-squared output currents $\overline{i_{out,1}^2}$, $\overline{i_{out,2}^2}$, and $\overline{i_{out,3}^2}$ and can be written as:

$$\overline{i_{out}^2} = \overline{i_{n,s}^2}\left(\frac{g_{m1}R_0}{s^2C_{gs1}(L_G+L_S)+s(C_{gs1}R_0+g_{m1}L_S)+1}\right)^2 + \overline{i_{n,d1}^2} - \overline{i_{n,d1}^2}\left(\frac{sg_{m1}L_S}{s^2C_{gs1}(L_G+L_S)-s(C_{gs1}R_0-g_{m1}L_S)+1}\right)^2 + \overline{i_{n,rl}^2}. \tag{3.15}$$

Using (3.12) and (3.15) the noise figure of the traditional LNA can be written. Fig. 15 and Fig. 16 show the normalized noise figure as a function of frequency and values of the inductors L_G and L_S. In Fig. 15, L_G has a negative impact of the noise figure at higher frequencies with large inductance values. On the other hand, the noise figure seems to be unaffected and even reduced by L_S values. From the figures, the inductor L_G is the significant contributor in shaping the noise figure, as well as the center frequency of the LNA. Using these plots, the inductor values can be selected to give the best noise figure performance for LNA.

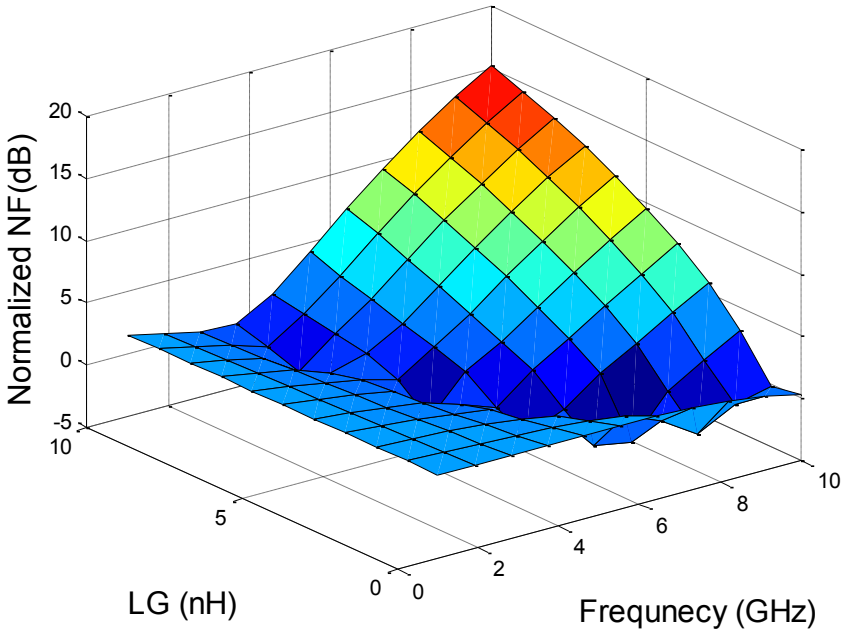

Fig. 15. Normalized noise figure plotted versus frequency and gate inductance, L_G.

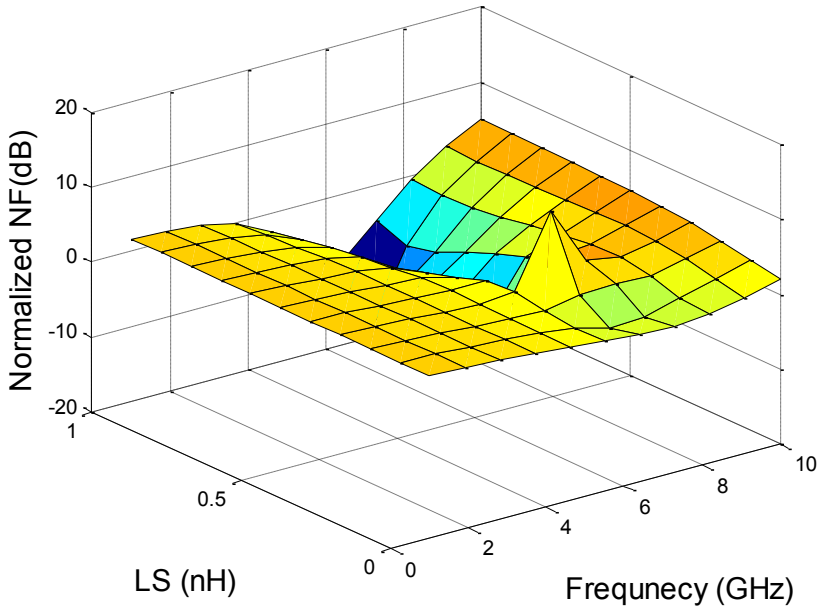

Fig. 16. Normalized noise figure plotted versus frequency and source inductance, L_S.

3.1.3 Linearity

Linearity issues arise when multiple signals are present, which can cause the system to become non-linear. A non-linear LNA is problematic as it causes non-linearities, such as gain compression, blocking, and intermodulation of the received signals. Common ways to quantify these non-linearities are 1-dB compression point ($P_{1\text{-dB}}$) and input-referred third-order intercept point (P_{IIP3}), normally expressed in dBm and desired to be as high as possible. Consider the linearity of a cascaded system shown in Fig. 17, where *x(t)* is the input signal, $y_1(t)$ is stage 1 output, $y_2(t)$ is stage 2 output, and IIP_3 is the third order input-referred intercept point of the stages. The overall system linearity in Fig. 17 is:

$$\frac{1}{A_{IIP3}^2} = \frac{1}{A_{IIP3,1}^2} + \frac{\alpha_1^2}{A_{IIP3,2}^2} \tag{3.16}$$

where α_1 is the small signal gain of stage 1. As the α_1 increases, the overall system's linearity decreases. Similarly, if (3.16) is expanded to *m* stages, the equation becomes:

$$\frac{1}{A_{IIP3}^2} = \frac{1}{A_{IIP3,1}^2} + \frac{\alpha_1^2}{A_{IIP3,2}^2} + \cdots + \frac{\alpha_1^2 \ldots (\alpha_{m-1})_1^2}{A_{IIP3,m}^2} \tag{3.17}$$

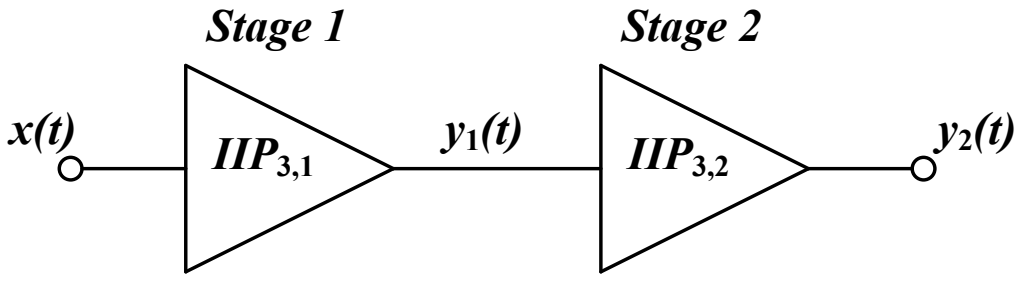

Fig. 17. Cascade of two linear stages.

From (3.17), the linearity of any given stage is scaled down by the gain of the preceding stages. Also from (3.17), the overall linearity is dominated by the latter stages. Regardless of the receiver's linearity, the linearity of the LNA is important to avoid placing challenging design requirements of following stages.

3.1.4 Gain

Gain is the ability to increase the power or amplitude of a signal from the input to the output of a circuit. Gain is expressed as:

$$A_P = \frac{P_{out}}{P_{in}},\ A_V = \frac{V_{out}}{V_{in}},\ A_i = \frac{i_{out}}{i_{in}} \tag{3.18}$$

where A_P is power gain, A_V is voltage gain and A_i is current gain. Gain, like noise, can be expressed in units of decibels (dB):

$$A_P = 10\log_{10}\left(\frac{P_{out}}{P_{in}}\right),\ A_V = 20\log_{10}\left(\frac{V_{out}}{V_{in}}\right),\ A_i = 20\log_{10}\left(\frac{i_{out}}{i_{in}}\right) \tag{3.19}$$

High gain is a desirable characteristic of any amplifier, including the LNA. From the previous analyses, it is seen that high gain is needed to lower the total noise figure while low gain is needed to increase total linearity for a multi-stage receiver.

The voltage gain of the conventional LNA can be expressed by the well-known equation:

$$A_V = G_M R_{out}, \tag{3.20}$$

where G_M is the effective transconductance of the LNA at its resonant frequency (see (3.2)). The input impedance network has a network Q, quality factor, since it resonates. The effective transconductance is dependent on the Q of the input impedance network:

$$G_M = 2Q_{in}g_m, \tag{3.21}$$

where Q_{in} is:

$$Q_{in} = \frac{1}{\omega_o(R_o C_{gs1} + g_{m1} L_S)} = \frac{\omega_o(L_S + L_G)}{R_o + \frac{g_{m1} L_S}{C_{gs1}}}. \quad (3.22)$$

Substituting (3.21) and (3.22) into (3.20), the voltage gain of the LNA can now be expressed as:

$$A_V = \frac{s g_{m1} g_{m2} L_L}{(1 + s^2 C_{gs1}(L_G + L_S) + s g_{m1} L_S)(g_{m1} + C_{gs2})}. \quad (3.23)$$

From (3.23), the gain is determined by the transconductance of M_1 and M_2, and the output resistance, which is the impedance of L_L.

3.1.5 Power Consumption and Area

Power consumption is another parameter that needs to be considered. Increased incorporation of RF systems into hand-held devices makes it essential to minimize power consumption in order to maximize battery life [44]. With each new technology node, the minimum feature size in CMOS processes is constantly being reduced, therefore area consumption is also an essential parameter.

The design of a LNA is a multi-dimensional optimization problem. There are numerous limitations and trade-offs involved, noise versus linearity, gain versus noise, area and power consumption, and the optimization of each metric does not have the same design solution.

3.2 Magnetically Tunable Matching Network

The design challenge of an input tunable LNA is finding an approach to reconfigure the input impedance network of the system in Fig. 1. From the impedance analysis, it is derived

from (3.1) and (3.2) that the inductor L_G determines the resonant frequency of the impedance match. Therefore, L_G must be tunable for the LNA to achieve frequency variation at the input. Several methods for realizing tunable inductors have been proposed, primarily in the context of voltage-controlled oscillators. These techniques consist of switched inductors, MEMS-based variable inductors, active inductors, and transformer-based variable inductors.

Switched inductors [45] and [46] operate by using one or more switches to selectively add or remove inductance from the signal path. This method is simple to implement, but due to the non-zero ON resistance of the switch, switched inductors suffer from degraded Q thus making them less suitable for use in LNA input matching networks. Commonly implemented via transistors, the switches also introduce noise into the signal path, thus increases the noise figure.

The inductance can also be controlled by changing the concentration of the magnetic flux lines in the inductor. This is the approach that is taken in MEMS-based variable inductors [47]. These inductors consist of a traditional integrated inductor and a metal or ferromagnetic plate which is placed above the inductor. By moving the position of the plate, the series inductance can be controlled. Unfortunately this requires a mechanical movement of the plate, which is not suitable for typical CMOS processes. An approach that is similar to switched inductors, but that does not suffer from the adverse effects of the switch was proposed in [48] and is referred to as a variable bridge inductor. The variable bridge inductor uses a bridge circuit with an array of MOSFET switches tapping the inductors at various balance points. With various combinations of switches, the series inductance can be

controlled. However this approach requires multiple switches thus introduces multiple noise sources into the signal path and degrading the noise figure.

Active inductors remove the inductor completely. Active inductors [49] and [50] use a combination of transistors, capacitors, and feedback to approximate the impedance and frequency response of an inductor. This method can achieve very small area and a wide range of inductance values, but the active component generates noise and, like the switched inductor, is less suitable for use in LNA input matching networks.

One realization of a transformer-based variable inductor consists of two coupled inductors which have constant inductance. When the series resistance of the secondary winding is changed by a switch, the magnetic field around the primary winding is altered through the mutual inductance. Through this technique, the effective inductance of the primary winding can be varied [51], [52]. The tuning range of this type of transformer-based inductor is dependent upon the coupling coefficient, k. Because k of integrated transformers is degraded by the loss resulting from the high-conductivity substrate, the tuning range tends to be only about 50% [48]. The problem of limited tuning range can be mitigated by using the magnetic tuning principle.

A magnetic tuning principle was introduced in [53] as a means for increasing the tuning range of voltage-controlled oscillators (VCO). By controlling the amplitude and phase of the currents through the windings of a transformer, the resonant frequency of a transformer-based tank can be varied. The resonator proposed in [53] is analyzed and explored as the possibility to realize a tunable matching network that is suitable for use in reconfigurable,

multi-band LNAs [54]. The schematic of a transformer-capacitor (TC) network is shown in Fig. 18 where R_P and R_2 model the loss of L_1 and L_2, respectively.

The voltage across the primary winding, L_1, can be expressed as:

$$V_1 = j\omega L_1 i_1 + j\omega M i_2 = -\frac{i_1}{j\omega C} \tag{3.24}$$

where M is the mutual inductance and i_1 and i_2 are the primary and secondary winding complex currents, respectively. From (3.24), the resonant frequency of this network can be found to be:

$$f_0 = \frac{1}{2*\pi\sqrt{C(L_1 \pm \alpha M)}} \tag{3.25}$$

where $\alpha = i_2/i_1$. By forcing the complex currents i_1 and i_2 to be either in phase or out of phase, α will be real and positive (for i_1 and i_2 in-phase) or real and negative (for i_1 and i_2 out of phase). Assuming that α is purely real, it can be seen from (3.25) that the resonant frequency can be varied simply by changing the relative magnitudes of the complex currents i_1 and i_2.

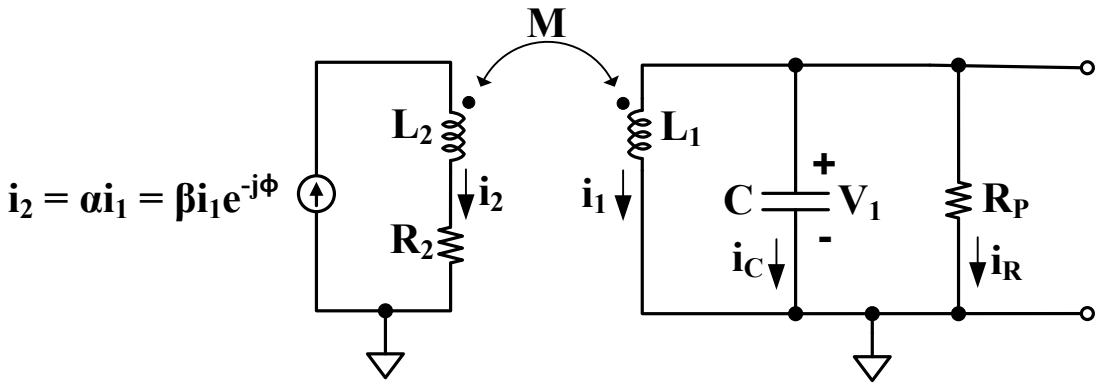

Fig. 18. Transformer-capacitor (TC) network.

This can be equated to varying the inductance of the primary winding, L_1, and this technique can be applied to realize a reconfigurable input matching network for LNAs.

Also from (3.25), it is seen that for some values of α, the term $L_1 \pm \alpha M$ can approach zero and become negative. At these points, the analysis in the subsequent discussions is no longer valid and the network enters an undefined region of operation. To avoid this condition, the following condition must be maintained:

$$|\alpha| < \frac{L_1}{M}. \tag{3.26}$$

The major advantage of the TC network is that the tuning range is no longer solely dependent upon the coupling coefficient k [52]. From (3.25), the tuning range is now heavily reliant on the current ratio α, which is controlled and limited only by (3.26). With these characteristics, the effects of the loss from the high conductivity of the substrate [48], such as degraded k and limited tuning range, are negligible.

In (3.25) and (3.26) it is assumed that α is purely real, but it is important to examine the effects of phase mismatch between the currents i_1 and i_2. Therefore i_2 is defined to be:

$$i_2 = \beta i_1 e^{-j\varphi} \tag{3.27}$$

where β is the gain and φ accounts for possible phase mismatches between the currents i_1 and i_2. Substituting (3.27) into $\alpha = i_2/i_1$, α is now defined to be:

$$\alpha = \beta e^{-j\varphi}. \tag{3.28}$$

When $\varphi = 0°$, i_1 and i_2 are in phase and that α is positive. Using this definition, the input impedance of the TC network shown in Fig. 18 can be expressed as:

$$Z_{in} = \frac{j\omega L_1 R_P + j\omega\beta M R_P e^{-j\varphi}}{R_P - \omega^2 C L_1 R_P - \omega^2 \beta C M R_P e^{-j\varphi} + j\omega L_1 + j\omega\beta M e^{-j\varphi}}. \quad (3.29)$$

The preceding discussion assumes that α is purely real. It is necessary to investigate the effects of arbitrary phase differences between i_1 and i_2. The effects of α, φ and M on the behavior of the TC network are explored through simulation of (3.24)-(3.29) using MATLAB and Advanced Design System (ADS) [54]. To help illustrate the design trade-offs, the TC network shown in Fig. 18 is used with the following component values: $L_1 = L_2 = 1$ nH, $C = 1$ pF, and $k = 0.4$. Further it is assumed that $Q = 10$ for both the primary and secondary winding of the transformer. Fig. 19 shows the resonant frequency, f_o, of the TC network as a function of α. Sweeping α from -2 to +5, the TC network can be tuned from approximately 3 GHz to 11 GHz, respectively. It is important to recall (3.21) and so β is also constrained by (3.19) and so when $\beta = 2.5$ and $\varphi = 180°$, in this example, the term $L_1 + \alpha M$ (i.e., the denominator of (3.18)) is equal to zero and the TC network enters an undefined region of operation.

Fig. 20 shows the resonant frequency as a function of φ, for the case when $\beta = 1$. Sweeping φ from -360° to +360°, the TC network's resonant frequency increases from 4.23 GHz up to 6.45 GHz, reaching the peak frequency at $\varphi = 180°$. When $\varphi = 180°$, α changes from positive to negative and hence a maximum frequency shift is observed. A difference of about 2 GHz in the resonant frequency is seen. Therefore, when the currents in the windings are not perfectly in-phase, the resonant frequency deviates from the expected value for all values of β. For ±1% accuracy of the resonant frequency, in this case, the TC network can tolerate up to 30° of phase mismatch between i_1 and i_2, indicating good stability in the presence of PVT variations.

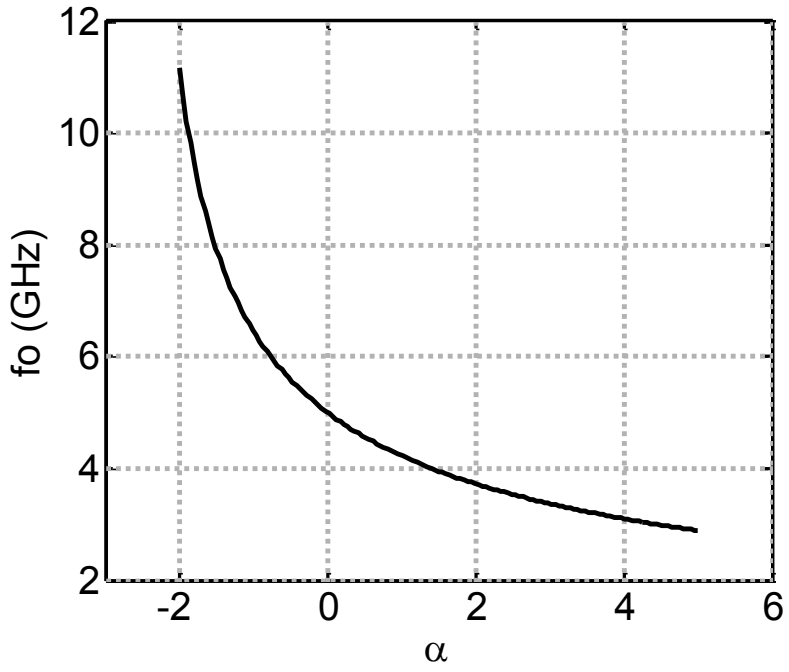

Fig. 19. Resonant frequency, f_o, as a function of α.

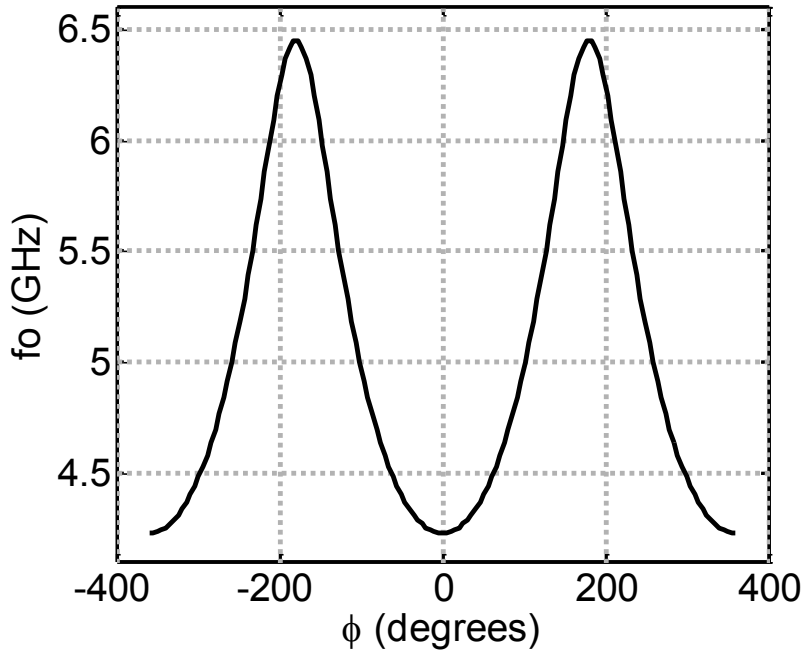

Fig. 20. Resonant frequency, f_o, as a function of φ, when $\beta = 1$.

For a general TC network, in order to achieve maximum frequency tuning, (3.25) indicates that k should be maximized ($M = k\sqrt{L_1 L_2}$). Having a large value for k (and in turn a large mutual inductance) increases the percentage change in the network's total inductance, allowing for a wide frequency tuning range. However, α must satisfy the condition set forth in (3.26) and arbitrarily increasing the coupling coefficient (and thereby M) will increase the minimum valid values for negative α. This is seen in Fig. 21 which shows the resonant frequency versus α, for different values of the coupling coefficient. It is seen that as k is increased, the value of α that results in the resonant frequency asymptotically approaching infinity increases. Since operation on the steep part of the curve is unwanted (due to poor control of the frequency in this range), the tuning range is effectively reduced.

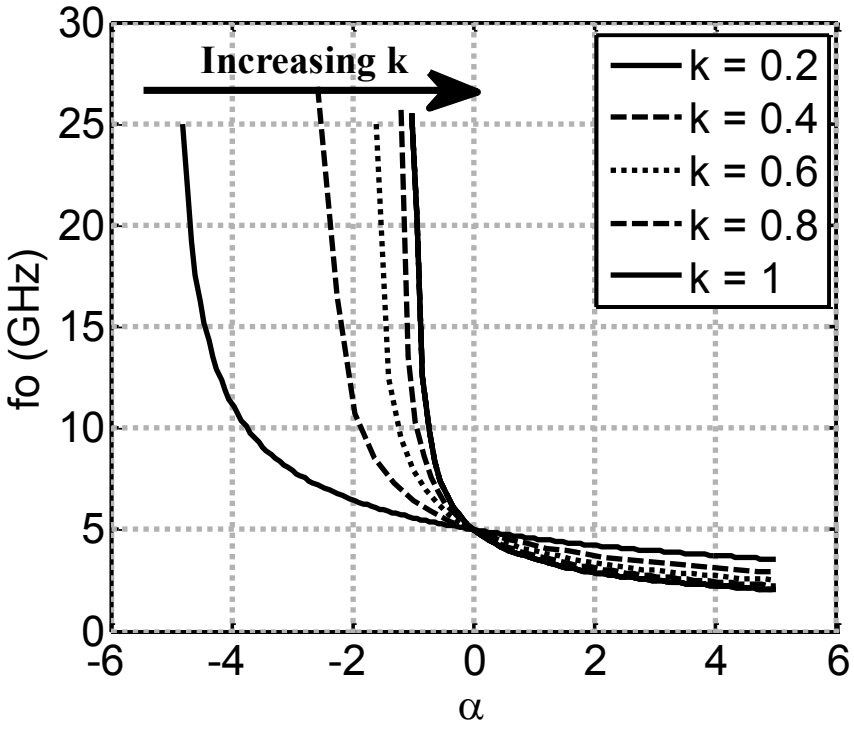

Fig. 21. Resonant frequency, f_o, as a function of α, while sweeping coupling coefficient, k.

In addition to a reduction in tuning range, an increased coupling coefficient also leads to an increased sensitivity to phase mismatches between i_1 and i_2. This is demonstrated in Fig. 22 which shows the resonant frequency as a function of φ for different values of k. As k increases, the variation in the resonant frequency also increases. It is seen that for $k = 1$, the maximum variation in the resonant frequencies is approximately 12 GHz. For ±1% accuracy of resonant frequencies, the TC network tolerates up to 30° of current phase mismatch. It is also worth looking at the lower frequency limit of the proposed TC matching network. Tuning to lower frequencies requires a larger inductance. Unfortunately, as the fixed inductance increases the percentage of the total inductance that is controlled by α is reduced thereby limiting the practical tuning range.

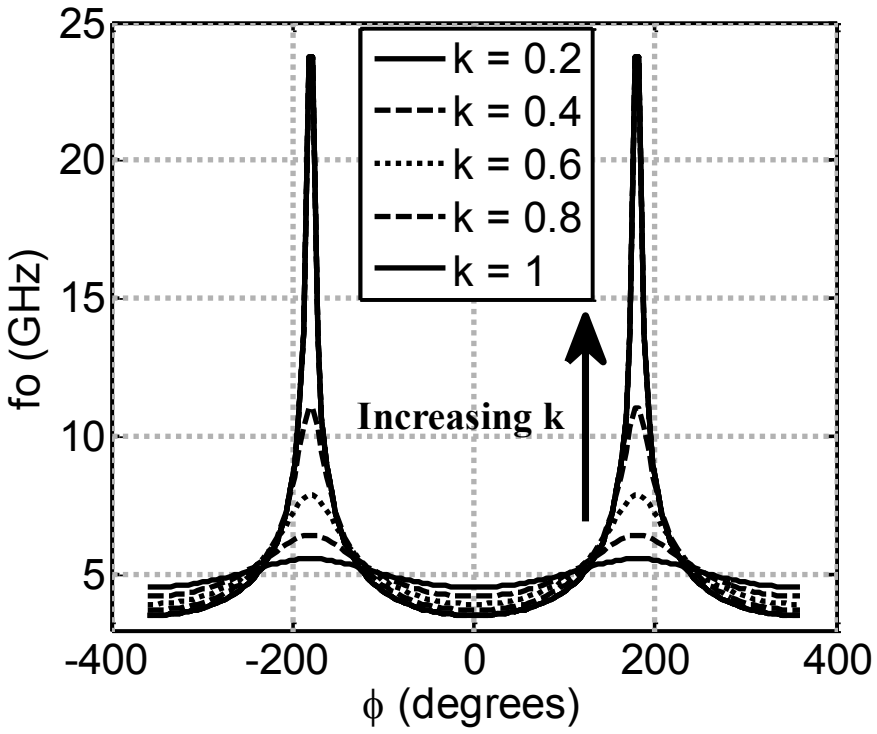

Fig. 22. Resonant frequency, f_o, as a function of φ, while sweeping coupling coefficient, k.

Finally, perhaps the most important characteristic of any matching network is its input impedance. Fig. 23 shows the real and imaginary impedance of the proposed TC network as a function of phase mismatch, φ for different frequencies of operation.

From Fig. 23, it is shown that proposed TC network achieves a real impedance of 50 Ω at both $\varphi = 0°$ and $\varphi = 180°$, but only purely real (Imag$\{Z_{in}\} = 0$) at $\varphi = 0°$. Also, the imaginary impedance is at its maximum for the different operation frequencies at $\varphi = 180°$, thus degrading the impedance matching of the TC network to the desired 50 Ω. Therefore, to achieve perfect input matching, the complex currents i_1 and i_2 should be in-phase or have a phase mismatch of $\varphi = 0°$.

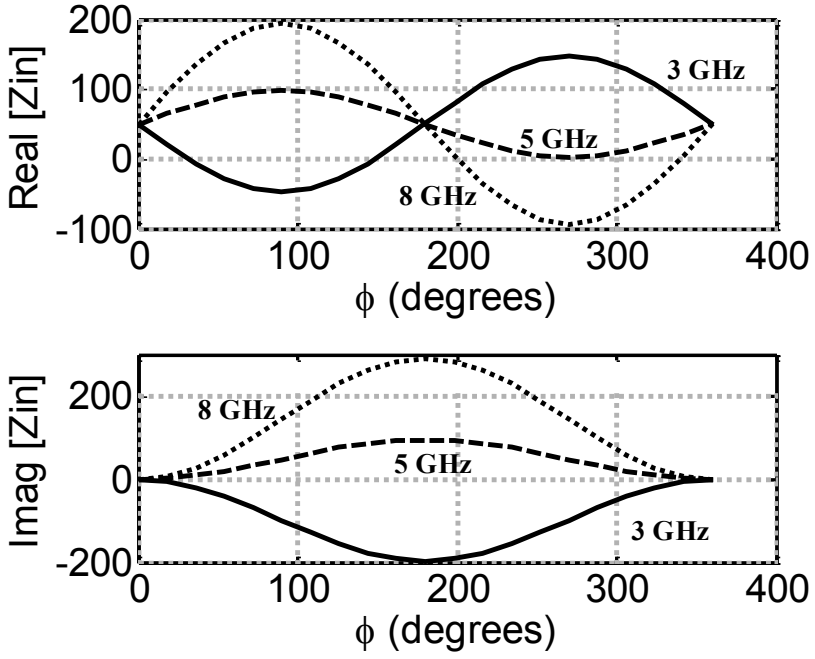

Fig. 23. Input impedance, Z_{in}, as a function of φ while sweeping frequency.

From the analysis of the transformer-capacitor (TC) network and the magnetic tuning principle, this technique has the capability to cover multiple bands and can be used for multi-band, multi-standard matching networks. This technique is implemented into the conventional narrow-band system to propose a new tunable LNA design, reconfigurable at the input.

3.3 Proposed LNA Design

In the previous sections, the traditional LNA metrics have been examined and the magnetic tuning principle was introduced and analyzed. The matching network technique has been implemented into the traditional common-source LNA, to propose a new reconfigurable LNA. The proposed tunable LNA is shown in Fig. 24. It is based on the traditional inductively degenerated LNA, but the gate inductor is replaced with the previously discussed transformer-based variable inductor (presented in [53]). Recall that for frequency tuning to occur, the currents in L_G and L_T must have a relative phase shift of either 0° or 180°.

One method for ensuring this condition is realizing that the output voltage of the LNA is simply an amplified, inverted version of the input voltage. By connecting the phase shifter to the output of M_1, between the cascode connection of M_1 and M_2 as shown in Fig. 24, the output voltage signal can be shifted and applied to the gate of transistor M_3. Transistor M_3 then converts the voltage signal to a current signal and applies it to the secondary winding of the input transformer. The magnitude of the current flowing through L_T can be controlled by varying the transconductance of M_3 which is accomplished by changing the DC bias voltage V_{TUNE}.

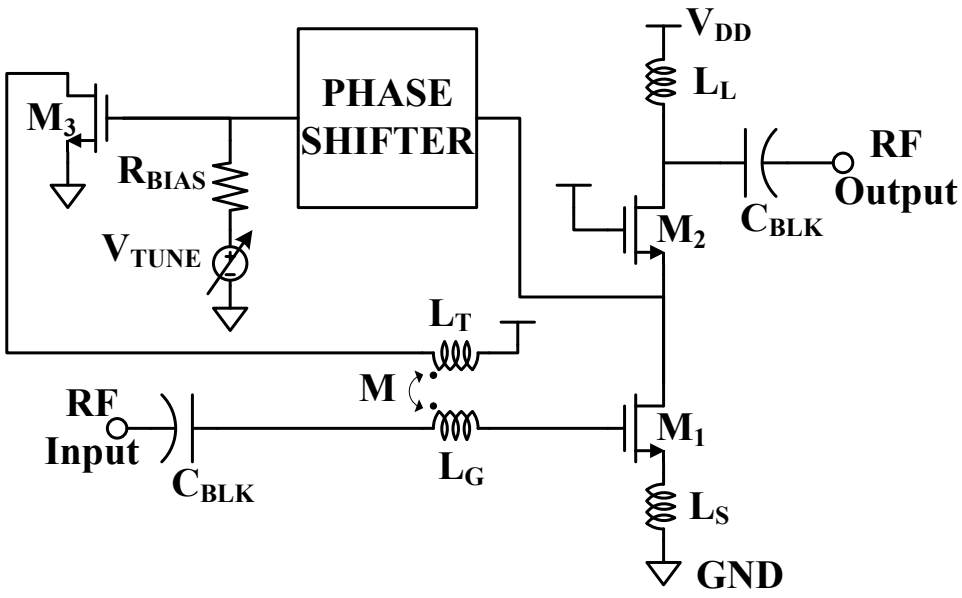

Fig. 24. Proposed tunable LNA.

3.3.1 Phase Shifter

A phase shifter is a complex design, capable of providing any amount of phase shift of an input signal. Several methods for realizing phase shifters have been proposed, these techniques consist of switched networks [55]-[59], hybrid designs [60], circulators [61]-[65], and variable resonant circuits [66]. An active phase shifter in [66] is designed to provide phase shift using a variable resonant circuit, providing over 100° of phase shift for a desired frequency bandwidth. The active phase shifter shown in Fig. 25 is implemented in the proposed LNA design [66]. The active phase shifter in Fig. 25 uses a cascaded connected common-gate transistor M_1 and common-source transistor M_2, and common-gate transistor M_3 in parallel. The variable resonant tank consisting of inductor L_P, capacitor C_P, and resistor R_P is placed in parallel, providing the phase shift via varying capacitance or inductance of the tank.

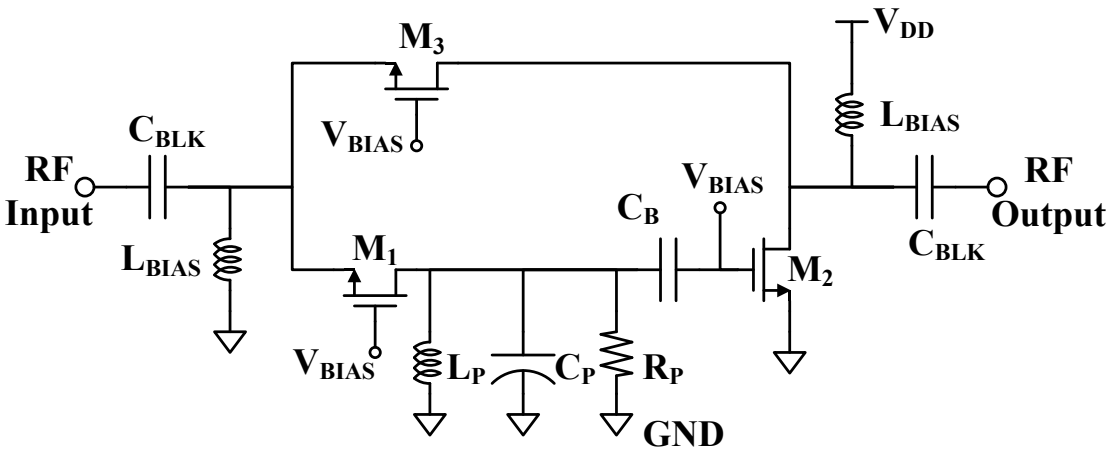

Fig. 25. Active phase shifter using a variable resonant circuit.

The advantages of this phase shifter are that input impedance matching is controlled by M_1 and M_3 transconductances and achieves over 100° of phase shift. Also, the phase can be changed with constant signal amplitude, therefore having low loss. The drawbacks include high power consumption, area consumption and high noise, as with most phase shifters. With the active phase shifter selected, the proposed LNA design is shown in Fig. 26. Now the performance metrics previously discussed must be reexamined in order to predict the effects that added circuitry of the proposed LNA will cause, in comparison to the traditional LNA.

3.3.2 Input Impedance

Input impedance is the first parameter to reexamine with the implementation of the magnetically tuned matching network, to determine if the impedance network is reconfigurable. The input impedance of the proposed LNA shown in Fig. 26 can now be written as:

$$Z_{in} = \frac{g_{m1}L_S}{C_{gs1}} + j\left[\omega(L_S + L_G \pm \alpha M) - \frac{1}{\omega C_{gs1}}\right] \tag{3.30}$$

where the frequency at which Z_{in} is purely real is now given to be:

$$\omega_0 = \frac{1}{\sqrt{C_{gs1}(L_S+L_G+\alpha M)}}. \tag{3.31}$$

$$Real\{Z_{in}\} = \frac{g_{m1}L_S}{C_{gs1}} \tag{3.32}$$

It can been seen in (3.30) and (3.32) that, like the traditional narrow-band LNA, the real part of Z_{in} is still determined by L_S only, while the operation frequency is determined by L_S and L_G. More importantly, however, is that the operation frequency now contains the term αM. Since α is controlled by varying the relative magnitudes of the currents in L_G and L_T, the operation frequency of the LNA can be controlled by simply varying V_{TUNE}. Thus the proposed LNA design is reconfigurable via the input impedance matching network.

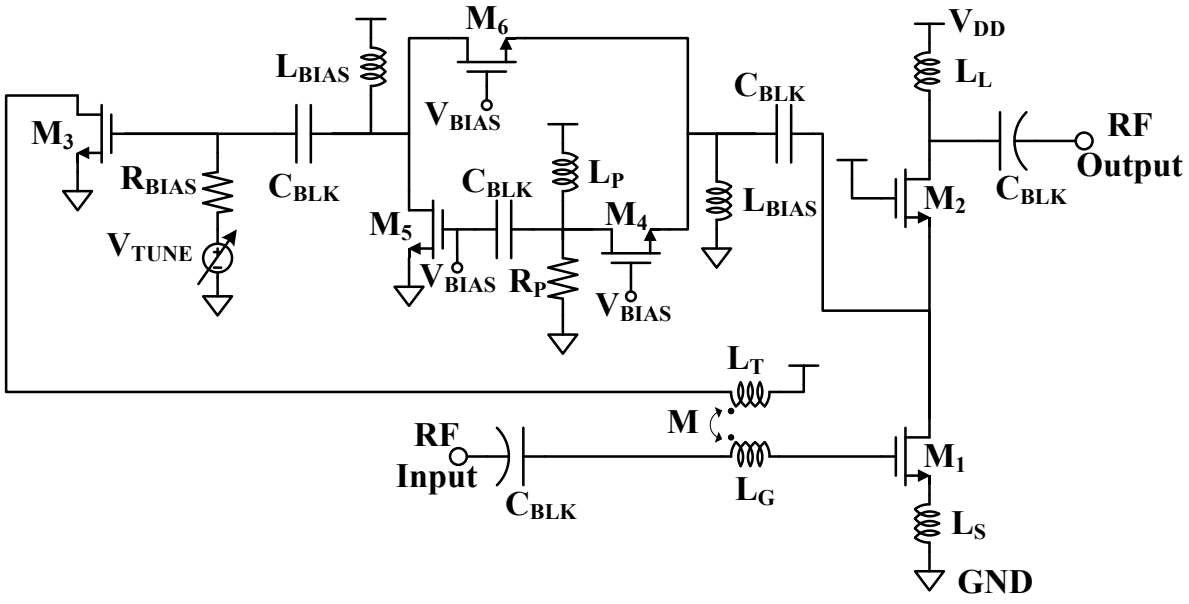

Fig. 26. Proposed LNA design with active phase shifter.

3.3.3 Gain

Gain of the proposed LNA shown can now be expressed as:

$$A_V = \frac{sg_{m1}g_{m2}L_L}{(1+ s^2C_{gs1}(L_G+ L_S\pm\alpha M)+ sg_{m1}L_S)(g_{m1}+C_{gs2})}. \quad (3.33)$$

From (3.33), the added circuitry does have an impact on the gain. Recall that the gain is shaped by the input impedance network, therefore as the new matching network's response changes, so will the gain's response.

Another important consideration is how the new tuning scheme will affect the overall noise figure of the LNA.

3.3.4 Noise Analysis

In the proposed design, the tuning circuitry is coupled to the input of the LNA through a transformer. In order to predict the effect that this will have on the overall noise figure, the short circuit output current for the system shown in Fig. 26 is derived. The equivalent circuit that is used for noise analysis is shown in Fig. 27. As previously mentioned, only thermal noise is considered and all inductors and capacitors are considered to be ideal.

The total short-circuit output noise current is comprised of effects from eight primary noise sources: noise from the source, $\overline{\iota_{n,s}^2}$, drain noise of M_1, $\overline{\iota_{n,d1}^2}$, drain noise of M_2, $\overline{\iota_{n,d2}^2}$, drain noise of M_4, $\overline{\iota_{n,d4}^2}$, drain noise of M_5, $\overline{\iota_{n,d5}^2}$, drain noise of M_6, $\overline{\iota_{n,d6}^2}$, thermal noise from the load resistor R_L, $\overline{\iota_{n,rl}^2}$, and drain noise from the tuning transistor M_3, $\overline{\iota_{n,d3}^2}$. Recall from previous noise analysis, it was assumed that M_2 did not significantly contribute to the total short-circuit output noise current (see (3.11)).

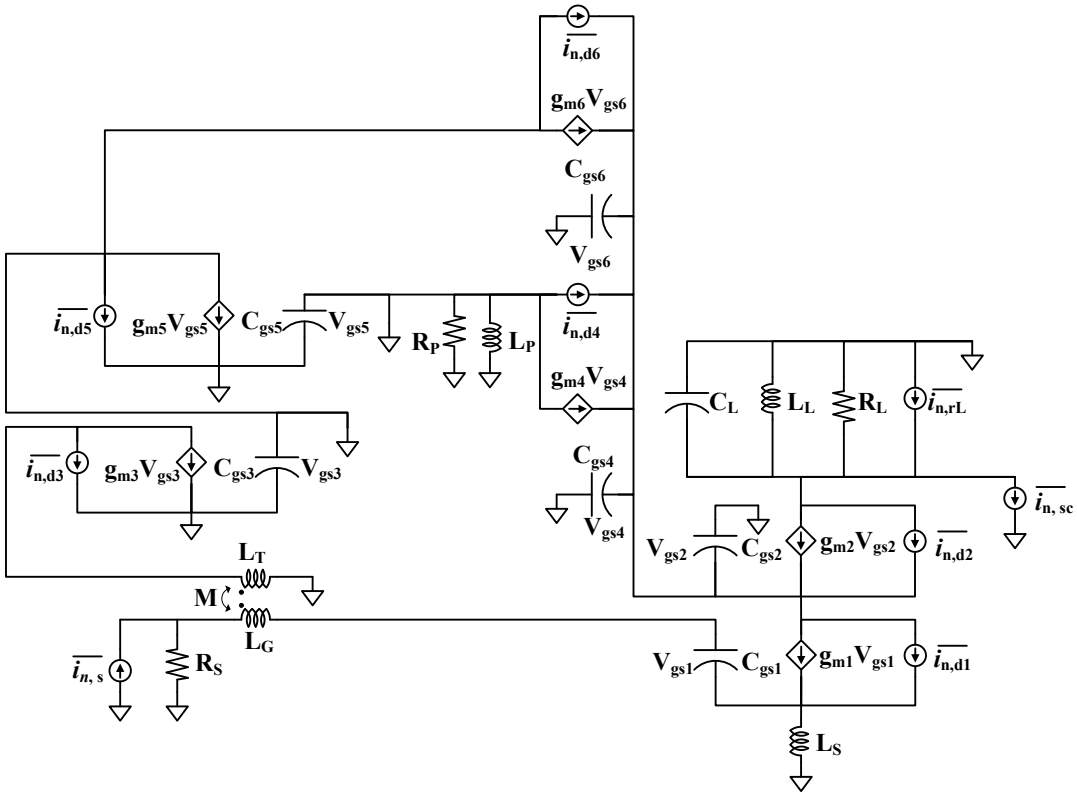

Fig. 27. Equivalent circuit used for noise analysis.

However, to accurately predict the effect of the phase shifter on the noise figure, M_2 is considered for this analysis. The input noise is shaped by the input matching network and is highly dependent on the network Q. An expression for the output noise current due to the source can be written as:

$$i_{out,1} = \left(\frac{g_{m1}R_S i_{n,s}}{1+s^2C_{gs1}(L_G+L_S)+s(g_{m1}L_S+C_{gs1}R_S)}\right)\left(\frac{-g_{m2}}{g_{m2}+g_{m4}+g_{m6}+sC_{eq}}\right). \quad (3.34)$$

where $C_{eq} = C_{gs2} + C_{gs4} + C_{gs6}$. The new expression $\frac{g_{m2}}{g_{m2}+g_{m4}+g_{m6}+sC_{eq}}$ comes from considering the effects of M_2, along with the phase shifter, on the overall noise figure. Next the driving transistor, M_1, is considered. As stated previously, only thermal drain current is

considered in this analysis and the short-circuit output noise current due to M_1 can be expressed as:

$$i_{out,2} = \left(i_{n,d1} - \frac{sg_{m1}L_S i_{n,d1}}{1+s^2C_{gs1}(L_G+L_S)+s(g_{m1}L_S+C_{gs1}R_S)}\right)\left(\frac{-g_{m2}}{g_{m2}+g_{m4}+g_{m6}+sC_{eq}}\right). \quad (3.35)$$

From (3.35), it is seen that the drain noise is also shaped by the input matching network. For the proposed LNA, like the conventional LNA, the primary contributor to the overall noise figure is the drain noise of M_1 [43].

The cascode common-gate transistor, M_2, is considered. An expression for the output noise current due to the due to M_2 can be written as:

$$i_{out,3} = i_{n,d2} - \frac{g_{m2}i_{n,d2}}{g_{m2}+g_{m4}+g_{m6}+sC_{eq}}. \quad (3.36)$$

From (3.36), it is seen that the drain noise of M_2, when considered, is also a significant contributor to the overall noise. Next the transistors M_4, M_5, and M_6 of the phase shifter are considered. An expression for the output noise current due to the M_4 can be written as:

$$i_{out,4} = \frac{-g_{m2}i_{n,d4}}{g_{m2}+g_{m4}+g_{m6}+sC_{eq}}. \quad (3.37)$$

An expression for the output noise current due to M_5 can be written as:

$$i_{out,5} = \frac{g_{m2}i_{n,d5}}{g_{m6}}. \quad (3.38)$$

An expression for the output noise current due to M_6 can be written as:

$$i_{out,6} = \frac{-g_{m2}i_{n,d6}}{g_{m2}+g_{m4}+g_{m6}+sC_{eq}}. \quad (3.39)$$

The noise for the load resistor R_L remains unchanged (see (3.14)), written as:

$$i_{out,7} = i_{n,rl}. \tag{3.40}$$

Finally, the effect of the tuning circuitry is considered. While it is assumed that the inductors are ideal with infinite Q, noise due to the finite Q of the inductor can simply be seen as increasing the noise current of M_3. By inspection of Fig. 27, the noise current from M_3 is magnetically coupled to the input of the LNA and is therefore shaped by the input network and scaled by g_{m1}. The short-circuit output noise current due to M_3 can be written as:

$$i_{out,8} = \left(-\frac{sg_{m1}Mi_{n,d3}}{1+s^2C_{gs1}(L_G+L_S)+s(g_{m1}L_S+C_{gs1}R_s)}\right)\left(\frac{-g_{m2}}{g_{m2}+g_{m4}+g_{m6}+sC_{eq}}\right). \tag{3.41}$$

Unlike the other noise current sources, the noise contribution from $i_{n,d3}$ can be minimized through optimization of the transformer design. It is seen in (3.41) that the noise current, $i_{out,3}$, is directly proportional to the mutual inductance, M, of the transformer and can therefore be minimized by minimizing M. This makes intuitive sense, because minimizing the coupling coefficient reduces the amount of noise that is coupled to the input of the LNA. Unfortunately, minimizing M, also reduces the overall tuning range (see (3.31)).

The total mean-squared noise current at the output of the LNA is simply the superposition of the individual mean-squared output currents $\overline{i_{out,1}^2}$, $\overline{i_{out,2}^2}$, $\overline{i_{out,3}^2}$, $\overline{i_{out,4}^2}$, $\overline{i_{out,5}^2}$, $\overline{i_{out,6}^2}$, $\overline{i_{out,7}^2}$ and $\overline{i_{out,8}^2}$ and can be written as:

$$\overline{i_{out}^2} =$$

$$-\overline{i_{n,s}^2}\left(\left(\frac{g_{m1}R_S}{1+s^2C_{gs1}(L_G+L_S)+s(g_{m1}L_S+C_{gs1}R_S)}\right)\left(\frac{g_{m2}}{g_{m2}+g_{m4}+g_{m6}+sC_{eq}}\right)\right)^2 - \overline{i_{n,d1}^2}\left(\frac{g_{m2}}{g_{m2}+g_{m4}+g_{m6}+sC_{eq}}\right)^2 +$$

$$\overline{\iota_{n,d1}^2}\left(\left(\frac{sg_{m1}L_S}{1-s^2C_{gs1}(L_G+L_S)+s(g_{m1}L_S+C_{gs1}R_s)}\right)\left(\frac{g_{m2}}{g_{m2}+g_{m4}+g_{m6}+sC_{eq}}\right)\right)^2+\overline{\iota_{n,d2}^2}-$$

$$\overline{\iota_{n,d2}^2}\left(\frac{g_{m2}}{g_{m2}+g_{m4}+g_{m6}+sC_{eq}}\right)^2-\overline{\iota_{n,d4}^2}\left(\frac{g_{m2}}{g_{m2}+g_{m4}+g_{m6}+sC_{eq}}\right)^2+\overline{\iota_{n,d5}^2}\left(\frac{g_{m2}}{g_{m6}}\right)-$$

$$\overline{\iota_{n,d6}^2}\left(\frac{g_{m2}}{g_{m2}+g_{m4}+g_{m6}+sC_{eq}}\right)^2+\overline{\iota_{n,rl}^2}+$$

$$\overline{\iota_{n,d3}^2}\left(\left(\frac{sg_{m1}M}{1-s^2C_{gs1}(L_G+L_S)+s(g_{m1}L_S+C_{gs1}R_s)}\right)\left(\frac{g_{m2}}{g_{m2}+g_{m4}+g_{m6}+sC_{eq}}\right)\right)^2. \quad (3.42)$$

Using (3.34) and (3.42) the noise figure of the proposed LNA can be written. The expression $\frac{g_{m2}}{g_{m2}+g_{m4}+g_{m6}+sC_{eq}}$ increases the noise figure, due to the zero introduced at $\omega_Z = \frac{g_{m2}}{g_{m2}+g_{m4}+g_{m6}+sC_{eq}}$. The zero ω_Z will cause the noise figure to increase at greater frequencies, $\omega > \omega_Z$, thus ω_Z should be maximized [41].

3.3.5 Stability

Stability is another design specification that needs to be closely inspected. Stability is a concern in the presence of feedback. These closed-loop systems may become unstable for certain combinations of source and load impedances at specific frequencies, thus oscillating at those unstable frequencies [42]. The proposed LNA in Fig. 26 has a feedback path, consisting of the phase shifter, tuning transistor M_3, and the transformer, from the output of M_1 to L_G.

There are three criteria that are used to characterize the stability of circuits: the Stern stability factor, K and Δ_S, the mu stability factor, μ, and phase margin, PM. Each of the factors can independently determine the stability of a system, all are not required. The Stern stability factor is defined as:

$$K = \frac{1+ |\Delta_S|^2 - |S_{11}|^2 - |S_{22}|^2}{2|S_{21}||S_{12}|} > 1, \tag{3.43}$$

$$\Delta_S = S_{11}S_{22} - S_{12}S_{21} < 1, \tag{3.44}$$

The criteria for (3.43) and (3.44) states that if $K > 1$ and $\Delta_S < 1$, then the circuit is unconditionally stable at the S-parameters frequencies, therefore the circuit does not oscillate. The μ stability factor is defined as:

$$\mu = \frac{1 - |S_{11}|^2}{|S_{22} - S_{11}^* \Delta_S| + |S_{12}S_{21}|} > 1, \tag{3.45}$$

where $\Delta_S = S_{11}S_{22} - S_{12}S_{21}$ and S_{11}^* is the complex conjugate of S_{11}. The criteria for (3.45) states that if $\mu > 1$, then the circuit is unconditionally stable. The problem with the stability equations (3.43) - (3.45) is they required S-parameters, which are difficult calculations, for a wide range of frequencies beyond the desired bandwidth.

Phase margin is defined as the difference between the loop-gain phase shift and -180° at the unity-gain frequency [67] and is expressed as:

$$PM = < LG(j\omega_t) - (-180°), \tag{3.46}$$

where LG is the loop-gain and ω_t is the unity-gain frequency, the frequency where $|LG| = 1$. The requirement for stability is that the |LG| curve must cross the 0 dB point, or equal 1, before the <LG reaches -180° [68]. Stability is guaranteed if the real part of the output or input impedance remains positive at all frequencies [42] for a fixed source or load impedance, respectively. In the case of the proposed LNA design, the real part of (3.5) must

abstain from being negative. Stability will be examined at the circuit-level simulations, along with linearity, area and power consumption.

The proposed LNA design can provide frequency variation via the input impedance network, using variable inductance via the magnetic tuning principle. Now that the analysis of the proposed tunable LNA has been derived, the proposed LNA can be designed using the explored insights and tradeoffs previously mentioned to achieve a system for the desired applications. The circuit level design and simulation results are discussed in the following chapter.

CHAPTER 4. CIRCUIT DESIGN AND SIMULATION

The proposed tunable LNA was designed in a commercially available 0.13µm CMOS process. The schematic of the proposed tunable LNA is shown in Fig. 28.

4.1 Proposed Tunable LNA Circuit Design

As previously mentioned, the proposed tunable LNA is comprised of the conventional inductively degenerated LNA core, an active phase shifter, tuning transistor M_3, and an output buffer for testing purposes. The core of the LNA is comprised of transistors M_1 and M_2, source inductor L_S, load inductor L_L, load resistor R_L, and load capacitor C_L. The transistors M_1 and M_2, the cascode structure, are sized to provide high transconductance and contribute minimum amounts of noise, while also offering great isolation between the input and output ports. The active variable phase shifter is designed to place the transformer's currents in phase via the variable resonant tank and transistors M_4, M_5 and M_6. The resonant tank uses a fixed inductor L_P and resistor R_P to generate the required phase shift and M_4 and M_6 are sized for impedance matching at the output of M_1, node connection between the cascode connection.

The sizing of the tuning transistor M_3 is also important. On one hand, maximizing the size of M_3 will increase the transconductance and thereby allow for a greater tuning range. On the other hand, a large transistor size means large noise contribution, which should be avoided. Transistor M_3 was sized to provide 10 mS of transconductance at a bias voltage of V_{TUNE} = 1.0 V, and turns on at a bias voltage of V_{TUNE} = 0.4 V. This value was determined through simulation to give the best trade-off between maximum tuning range and minimum overall noise figure.

4.2 Transformer Design

The custom transformer was designed using Agilent's ADS Momentum and is shown in Fig. 29. The inner inductor is the gate inductor L_G, the primary winding of the transformer. The outer inductor is the tuning inductor L_T, the secondary winding of the transformer.

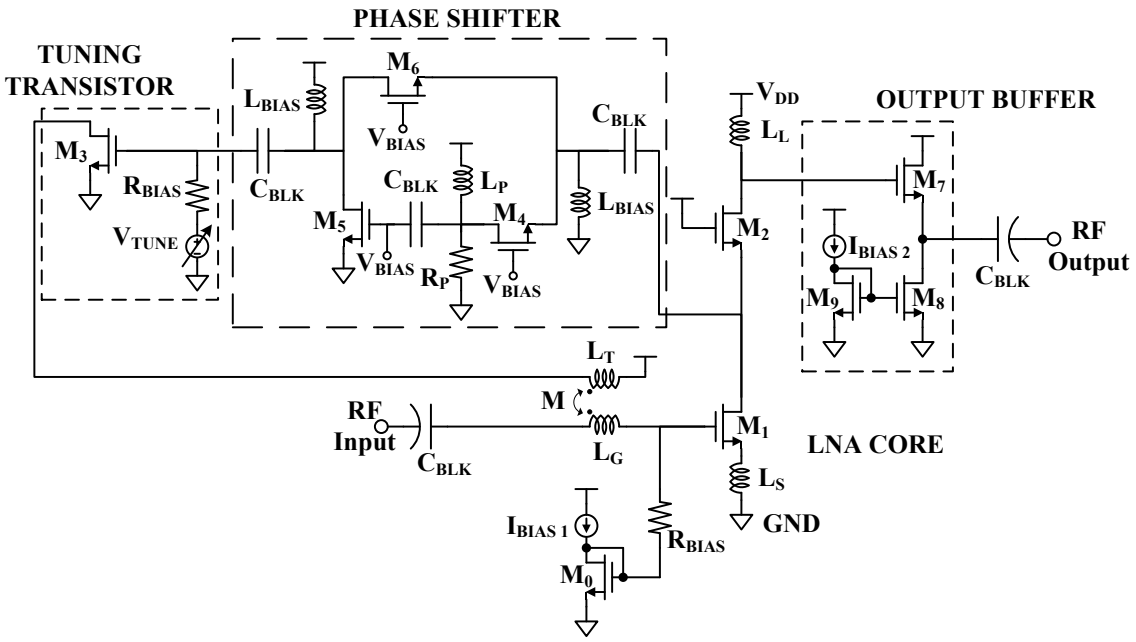

Fig. 28. Proposed tunable LNA design.

In order to achieve maximum tuning, from (3.24), k should be maximized ($M = k\sqrt{L_G L_T}$). Unfortunately, it was shown in (3.32) that maximizing k also increases the amount by which M_3 degrades the overall noise figure of the LNA. For these reasons a low value of $k = 0.2$ via the concentric structure is chosen for the input transformer.

The transformer was designed to have primary and secondary inductances, L_P and L_S, of 5 nH and 3 nH, respectively. To achieve desired k and inductance values, the lower inductance value was chosen as outer inductor and the higher value as the inner inductor. The outer inductor has an outer dimension of 290 µm and 2.25 turns to achieve a value of 3 nH, the inner inductor's outer dimension is 170 µm and 7.5 turns to achieve a value of 5 nH. The spacing between the inductors is at least 35 µm and the total area is 302 µm x 314 µm. The transformer design was extracted and simulated via ADS Momentum for verification of k, L_P and L_S. Figs. 30 and 31 show the effective inductances and coupling coefficient for the transformer.

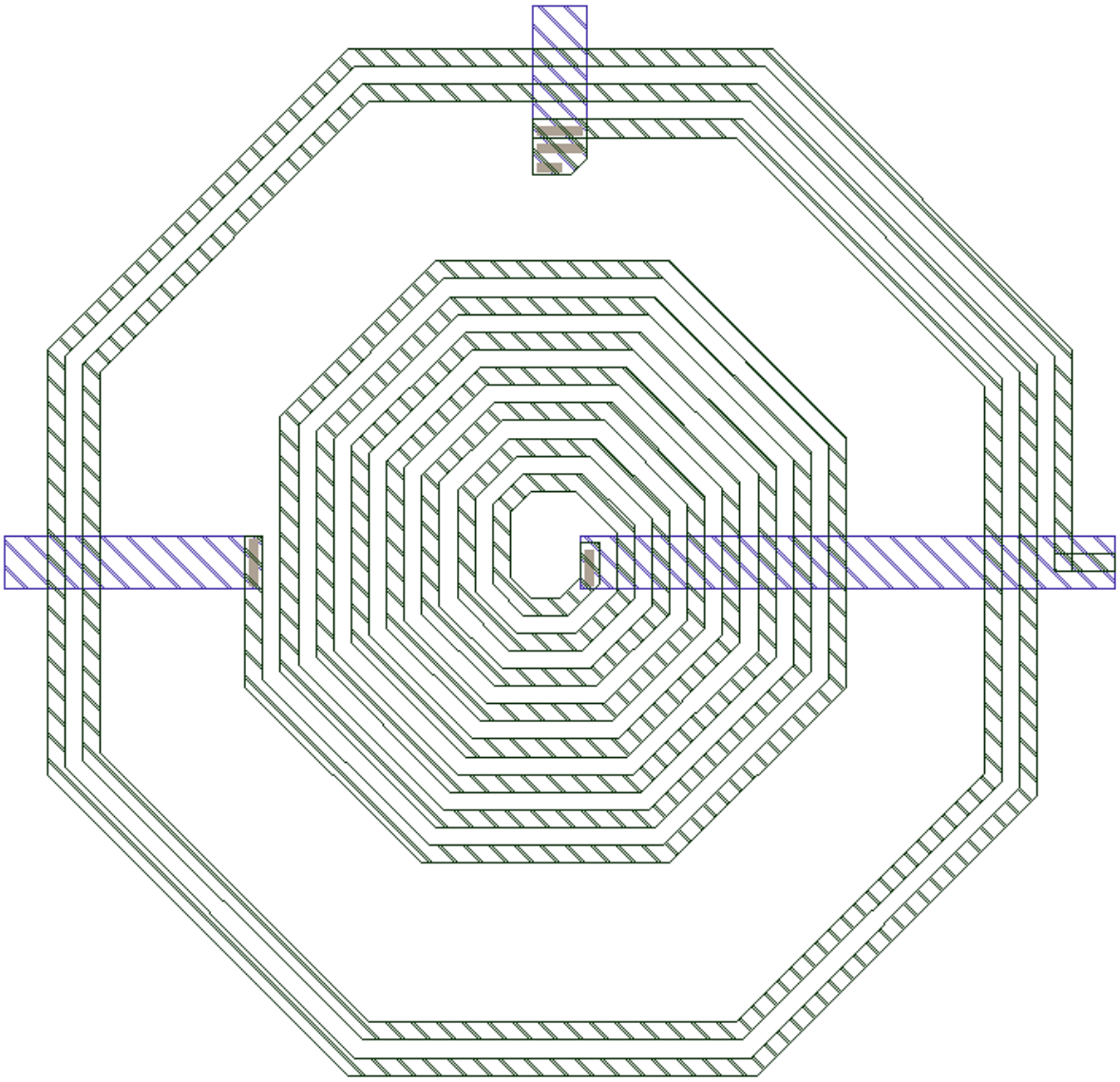

Fig. 29. Custom input transformer design.

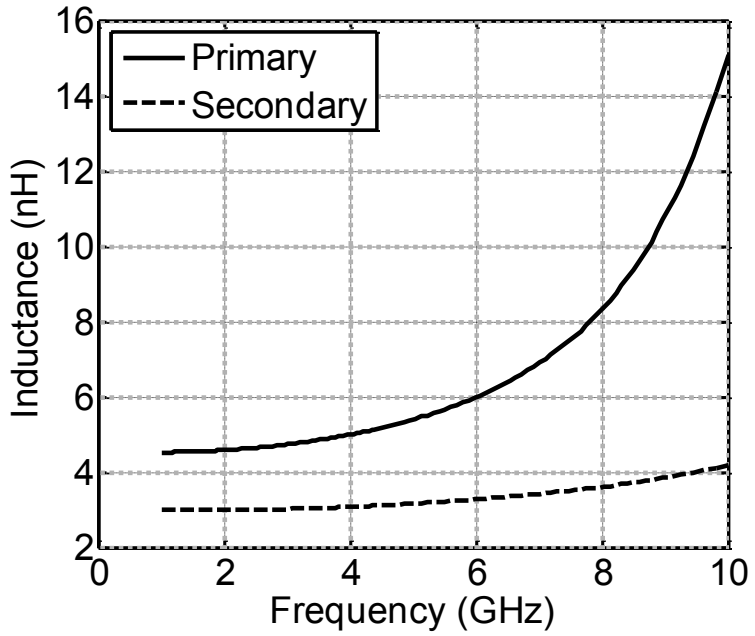

Fig. 30. Effective inductances of transformer as a function of frequency.

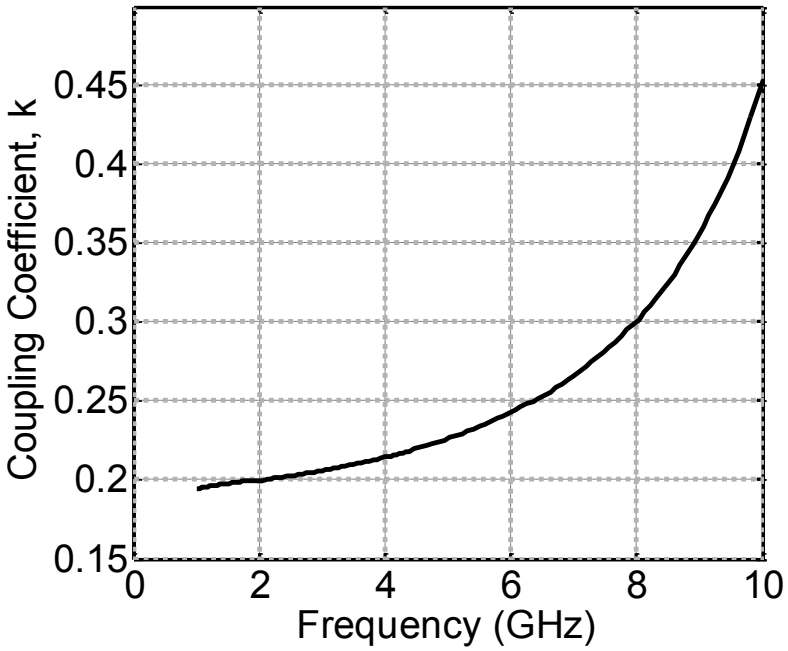

Fig. 31. Effective coupling coefficient *k* of transformer as a function of frequency.

In Figs. 30 and 31, it is seen that the desired values for the inductors and coupling coefficients are attained at frequencies lower than 6 GHz, then the values increase at higher frequencies. Now that the custom on-chip transformer is designed, a time-domain model is need for simulation of the proposed tunable LNA.

The transformer is characterized by two parameterized nine-component inductor models to account for the parasitics and used for simulation. The time-domain models are shown in Fig. 32, where L_P and R_P, and L_S and R_S are the primary and secondary inductances and series resistances, respectively. C_P models the parasitic capacitance of the inductors, C_{OX} models oxide capacitance, and the substrate capacitance and resistance are C_{SUB} and R_{SUB}. The time-domain models are used to match the 4- port S-parameters of the custom transformer in Fig. 29. Values for the components are found via ADS OPTIM function, which optimizes the components' values for matching. Table I displays the component values attained for good matching between the transformer and time-domain model. Figs. 33 through 36 display the S-parameter matching of the transformer and time-domain models. As shown in the figures, the matching of the each inductor is nearly perfect, such as S_{11}, S_{21}, S_{33} and S_{43}. The cross matching S-parameters, such as S_{13} and S_{24}, of the inductors has some deviations but is close enough to move forward with the simulation of the proposed tunable LNA.

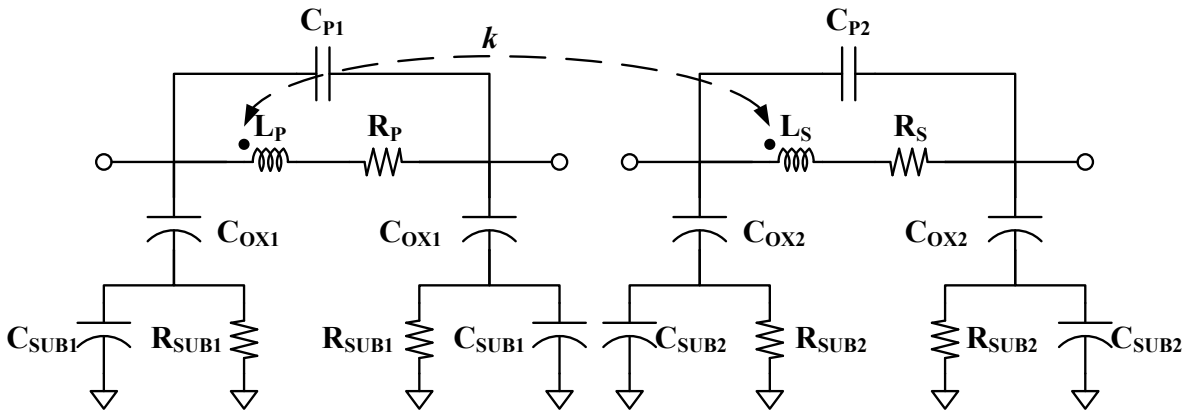

Fig. 32. Parameterized time-domain transformer model.

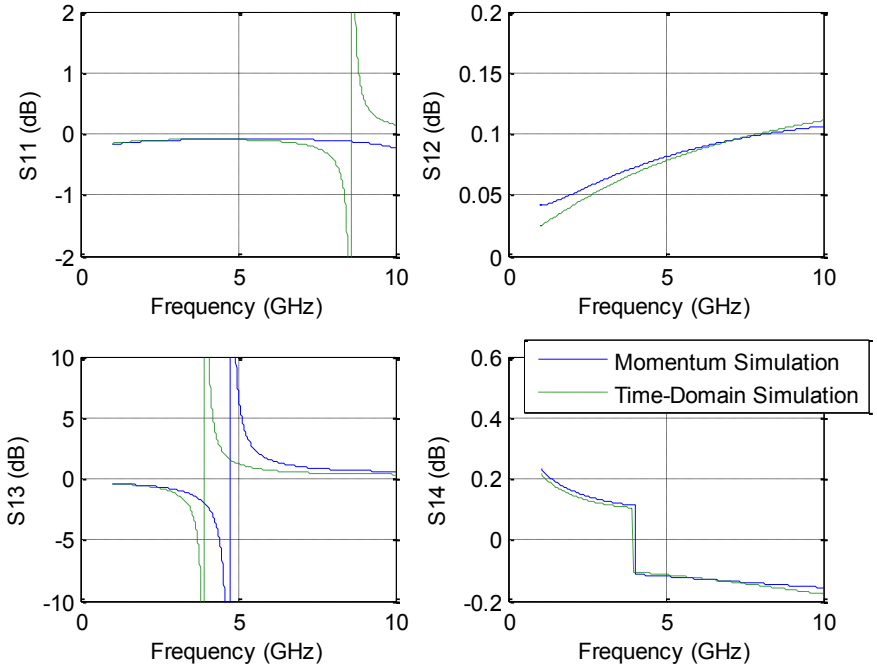

Fig. 33. Simulated S-parameter matching for Port 1.

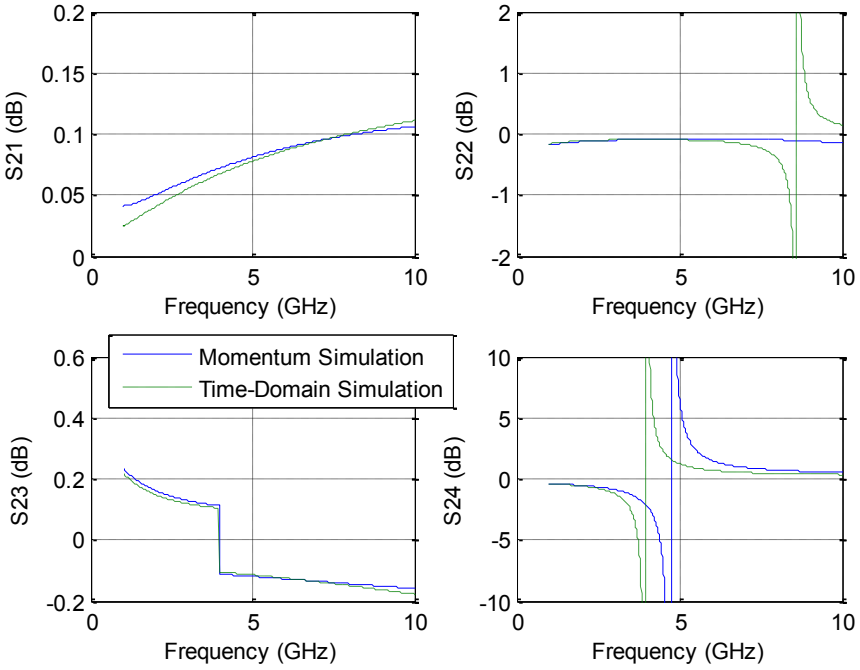

Fig. 34. Simulated S-parameter matching for Port 2.

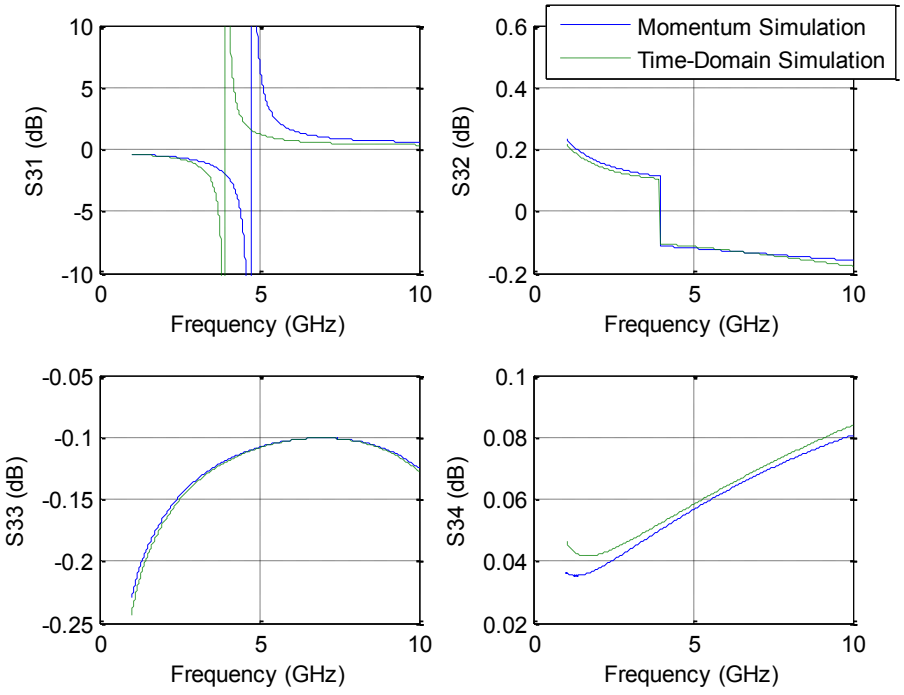

Fig. 35. Simulated S-parameter matching for Port 3.

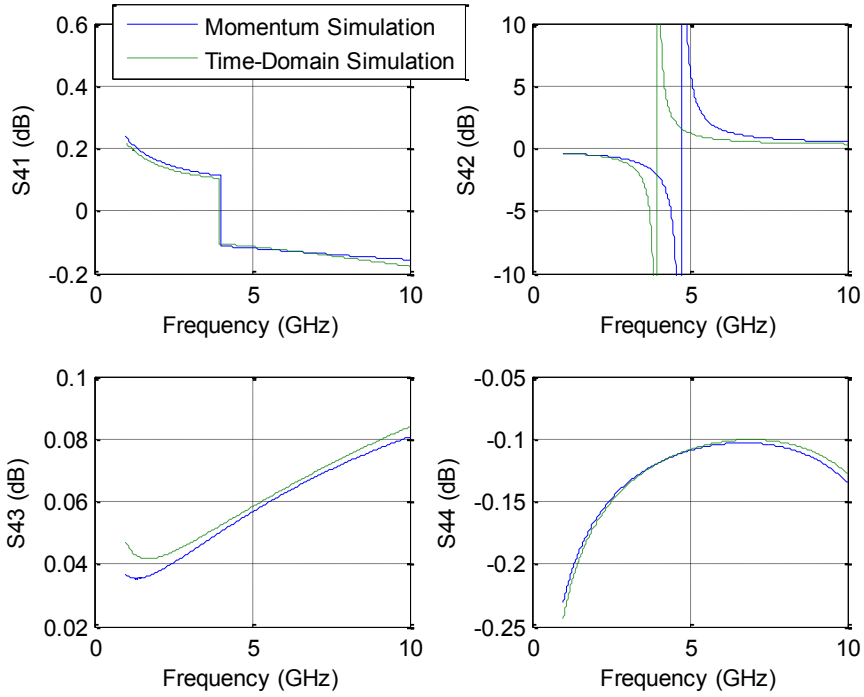

Fig. 36. Simulated S-parameter matching for Port 4.

TABLE I

TRANSFORMER TIME-DOMAIN MODELS COMPONENT VALUES

	L (nH)	R (Ω)	C_P (pF)	C_{OX} (fF)	C_{SUB} (fF)	R_{SUB} (Ω)	*k*
Primary	5	0.91	9.24e-4	77.3	340.157	49.98	0.23
Secondary	3	4.47	1.27e-9	47.2	0.05513	31.44	

4.3 Simulation Results

Simulations were performed and Fig. 37 shows the simulated S_{11} as a function of frequency for different values of V_{TUNE}. The operating frequency is taken as those frequencies for which $|S_{11}| < -10$ dB. By sweeping V_{TUNE} from 0–1.2 V, S_{11} can be tuned from approximately 3.2 GHz to 4.6 GHz, bandwidth of 1.4 GHz. The center frequency is taken as the frequencies for which $|S_{11}|$ is the minimum. Fig. 38 shows how the simulated gain, S_{21}, varies as a function of frequency for different values of V_{TUNE}. Across the tuning range, the gain stays relatively flat, with a 2 dB variation of the curves. Fig. 39 shows how the simulated gain, S_{21}, varies as a function of V_{TUNE}. This response is generated from the gain at the LNA's center frequency, where $|S_{11}|$ is minimum, which vary between 14.4–16.5 dB. From Fig. 39, the center frequency gain decreases as V_{TUNE} is increased.

The theoretical and simulated noise figures are shown in Figs. 40 through 42. Fig. 40 shows the compares the theoretical analysis and simulated noise figure of the traditional and proposed tunable LNA for the values of the proposed design. From Fig. 40, the theoretical noise analysis provides an accurate behavior prediction of the noise figure for the proposed tunable LNA.

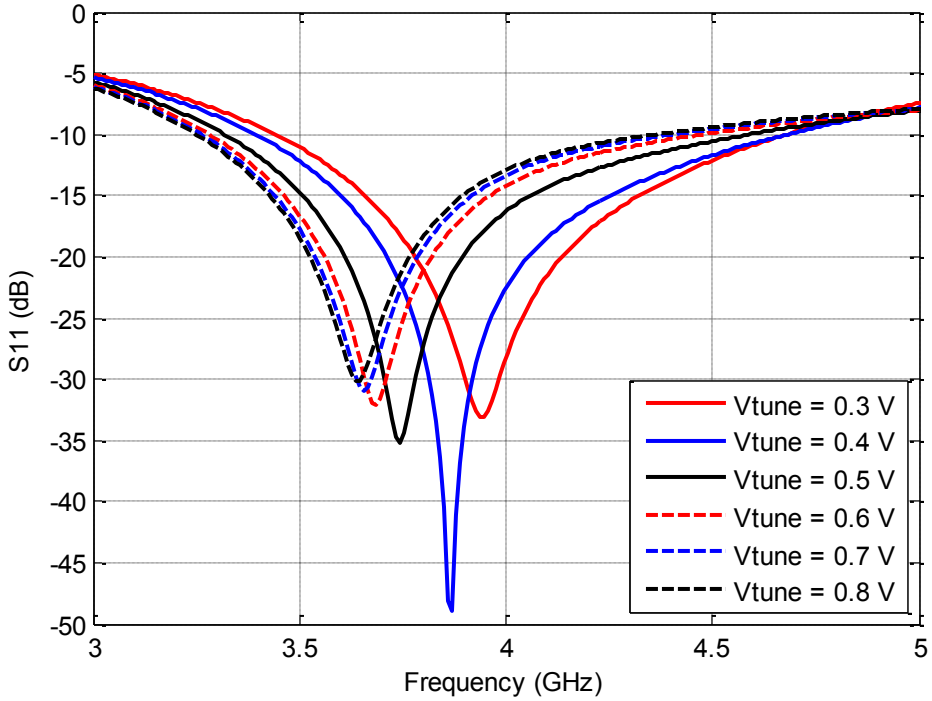

Fig. 37. Simulated S_{11} as a function of frequency for different values of V_{TUNE}.

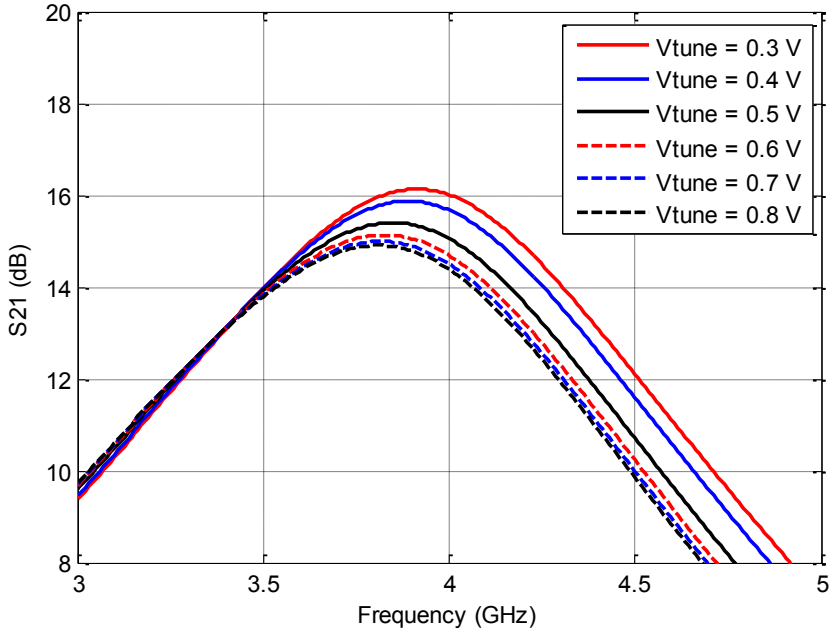

Fig. 38. Simulated S21 as a function of frequency for different values of V_{TUNE}.

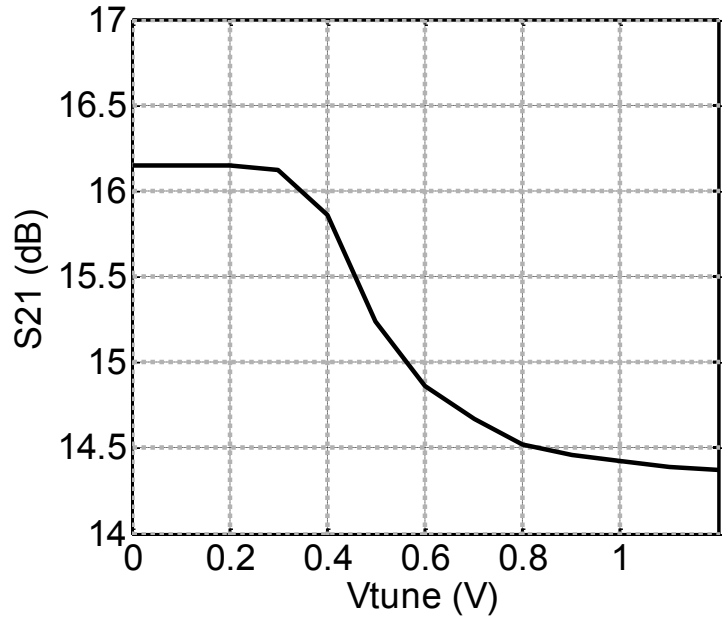

Fig. 39. Simulated center frequency S_{21} as a function of V_{TUNE}.

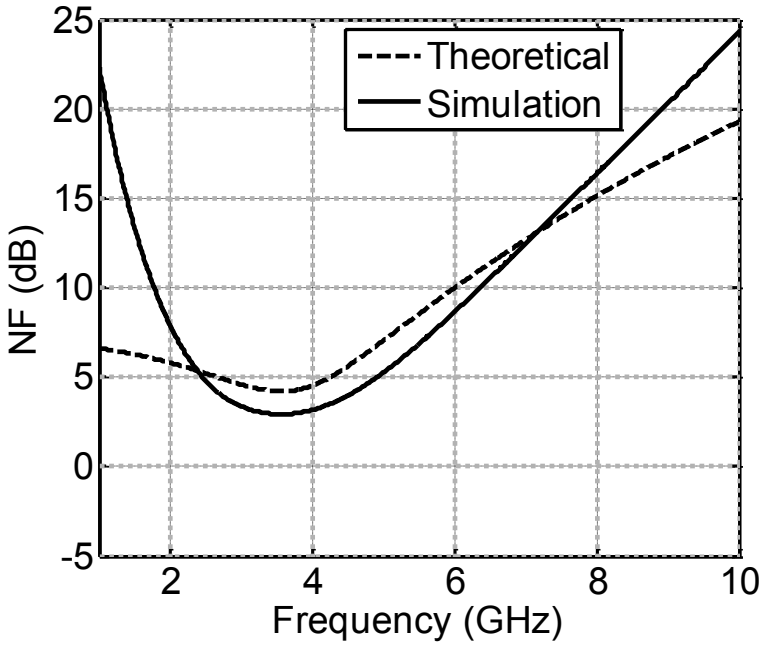

Fig. 40. Comparison of noise figure as a function of frequency.

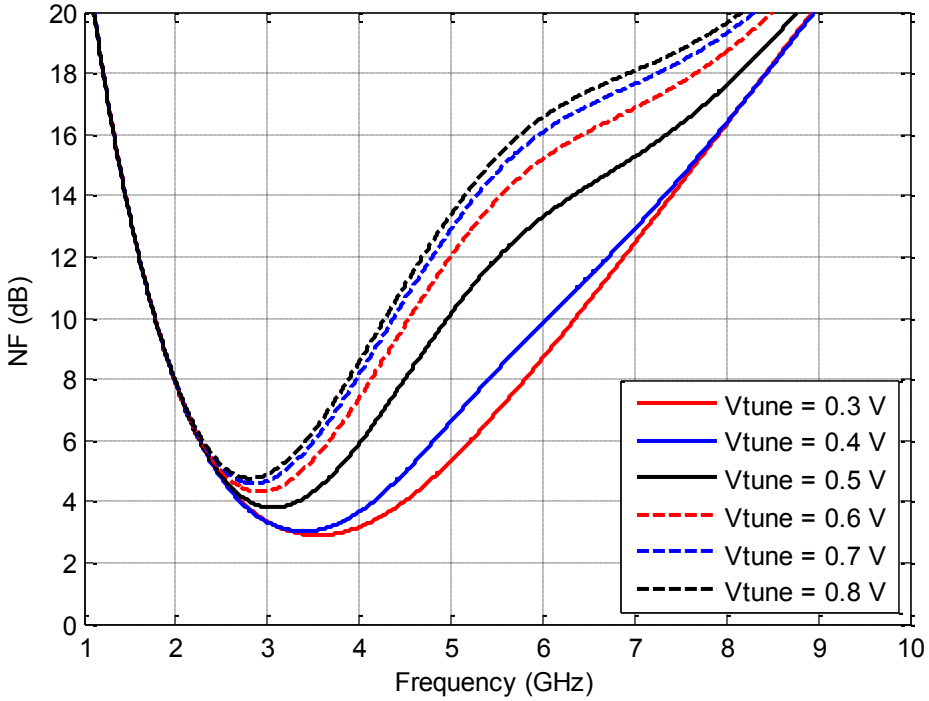

Fig. 41. Simulated noise figure as a function of frequency for different values of V_{TUNE}.

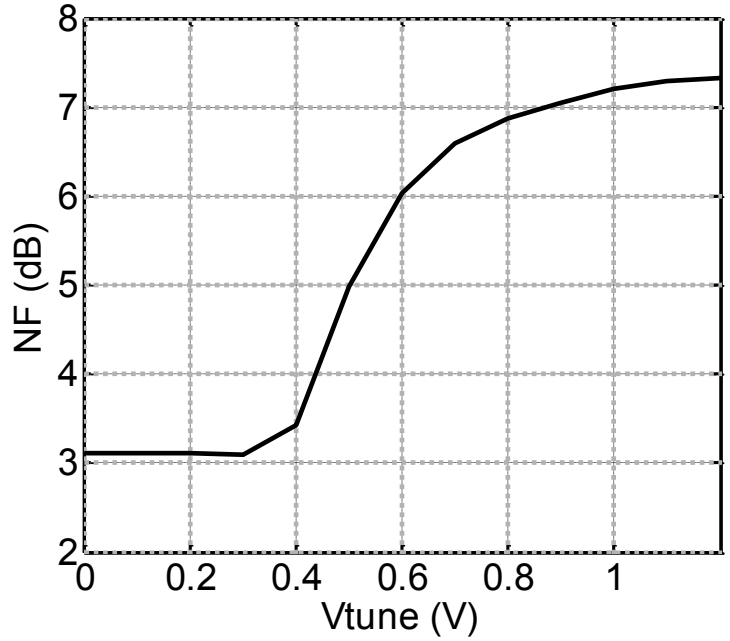

Fig. 42. Simulated center frequency noise figure as a function of V_{TUNE}.

Fig. 41 displays the simulated noise figure as a function of frequency for different values of V_{TUNE}. As V_{TUNE} increases, the noise figure over the tuning range increases also. Fig. 42 shows the simulated noise figure as a function of V_{TUNE}. This noise figure response is generated from the noise at the LNA's center frequency, where $|S_{11}|$ is minimum, which vary between 3.0–7.5 dB. Fig. 42 provides a better illustration of the effects of the tuning transistor M_3 on the noise figure. As V_{TUNE} is increased, the noise figure increases due to the power of the noise generated from M_3 increases. With these two major effects, the proposed tunable LNA has high noise figure, maximum at 7.5 dB.

Fig. 43 shows the simulated input third-order intercept (IIP3) as a function of V_{TUNE}. Two adjacent tones, the desired signal and blocker, with equal power are spaced by 20 MHz and fed into the proposed tunable LNA. The tested frequencies are set within the bandwidth for each V_{TUNE}, then the power of the signals is swept from -50 dBm to 0 dBm. From Fig. 43, the IIP3 ranges from -7.3 to -6.4 dBm, degrading as V_{TUNE} increases. The stability of the proposed tunable LNA is shown in Fig. 44 for varying V_{TUNE}. The mu factor, μ, is chosen from the three criteria to check for stability (see (3.45)), using the S-parameters acquired from previous simulations. As seen in Fig. 44, the proposed tunable LNA is greater than 1 at frequencies of interest and beyond, thus achieving stability while sweeping V_{TUNE}.

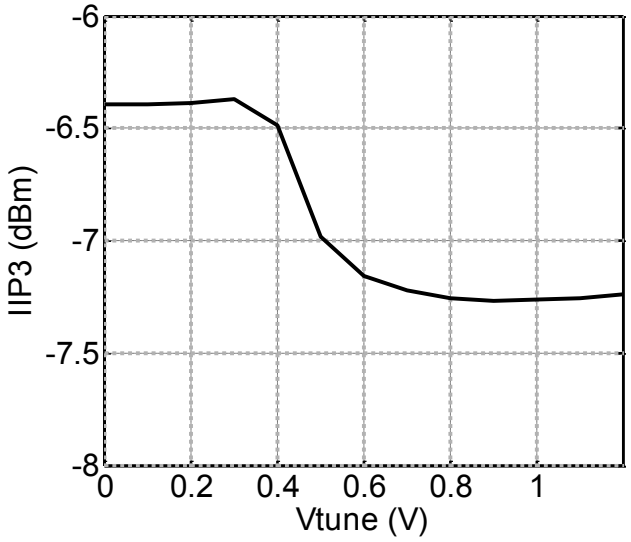

Fig. 43. Simulated IIP3 as a function of V_{TUNE}. Tone spacing is 20 MHz.

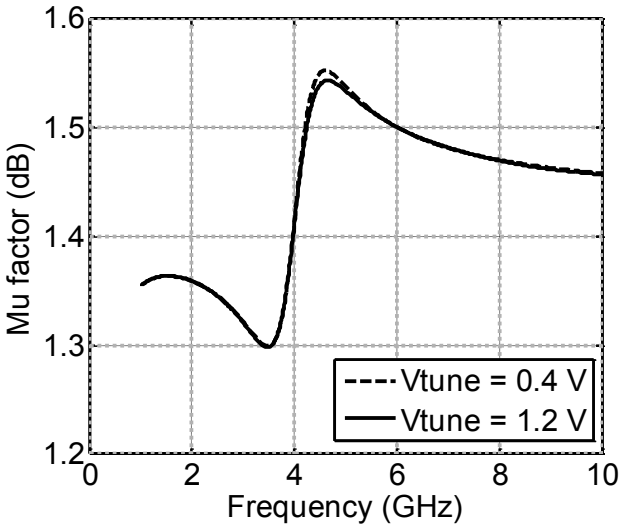

Fig. 44. Simulated stability as a frequency.

The proposed tunable LNA draws 42 mA from a 1.2 V supply resulting in a power consumption of 50 mW, neglecting the buffer required to drive the 50 Ω test equipment. Fig. 45 displays the breakdown of power consumption for the tunable LNA. It is seen in the figure the major contributor to the large power consumption is the active phase shifter, accountable for 67% of the total power consumed by the proposed tunable LNA.

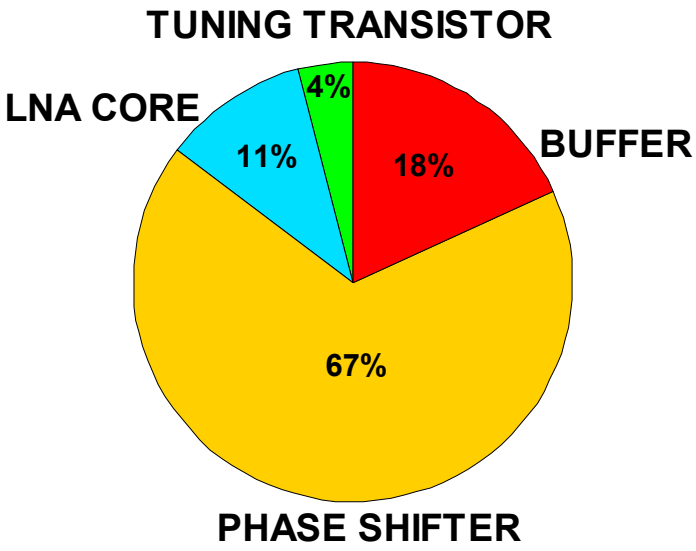

Fig. 45. Tunable LNA power consumption breakdown.

TABLE II

SUMMARY OF LNA PERFORMANCE AND COMPARISON TO PREVIOUSLY PUBLISHED DESIGNS

	Frequency Range (GHz)	S_{11} (dB)	Max S_{21} (dB)	Max NF (dB)	IIP3 (dBm)	Area (mm^2)	Power Consumption (mW)	Technology
[5]	2.3 – 9	< -9.9	9.3	9	-6.7	1.1	18	0.18 µm
[24]	2.5 – 4	< -10	19	5.4	-8	0.77	16	0.09 µm
[19]	0.1 – 6.5	< -10	19	4.2	N/A	N/A	12	0.13 µm
[17]	2.4 – 4.6	< -9	9.8	4	-7	0.9	16.2	0.13 µm
This Work	3.2 – 4.6	< -10	16.2	7.5	-6.4	N/A	50	0.13 µm

The performance of the proposed tunable LNA is compared with other similar, previously published LNAs in Table II. It is seen that the proposed system has the best linearity reported while also achieving competitive gain and tuning range. It is expected that the tuning range can be improved by utilizing a slightly higher coupling coefficient in future designs. The drawbacks, however, are the high power consumption and high noise figure. As mentioned earlier via analysis and simulation, the addition of the phase shifter is the significant contributor to the increase in noise figure and the high power consumption.

The system in [5] uses the *LC* bandpass filtering technique to achieve a wideband impedance match, [17] employs resistive feedback to generate the wideband frequency response. The systems [19] and [24] use common-gate inputs to attain its wideband impedance. While these systems have a wide tuning ranges, the drawbacks are undesired interferers are allowed to pass through and increased noise figure. With the proposed tunable LNA, the frequency response remains narrowband, naturally filtering interferers while maintain a competitive tuning range. While unknown, it can be expected that the area of the proposed tunable LNA will be competitive also.

CHAPTER 5. CONCLUSION

5.1 Future Work

The presented tunable LNA design will be fabricated in a commercially available 0.13µm CMOS technology and tested in the future. After measurements and comparative analysis of the presented tunable LNA, the designs of the stages following the LNA in the receiver chain will be considered. The basic RF receiver front-end architecture is shown in Fig. 46, the mixer, oscillator, low pass filter (LPF) and analog-to-digital converter (ADC) are the latter stages of the front-end RF receiver. With the tunable LNA capable of receiving multiple bands, these stages must also have similar broadband frequency responses, thus reconfigurable. In an effort to realize a future reconfigurable front-end receiver, its merits should be considered as they will guide the design of the remaining stages.

In a receiver, for good noise and linearity, more gain is needed in the earlier and latter stages, respectively. Therefore, the gain should be balanced throughout the system. The noise figure of the receiver is dominated by the first few stages, thus the LNA, mixer and oscillator should be designed for low noise figure. The linearity of the receiver is dominated by the latter stages, thus the LPF and ADC should be very design for high linearity. Each stage must be able to operate at any frequency within the desired range. In the future, research will focus on the reconfigurable designs of a mixer, an oscillator, LPF and ADC to fully realize a reconfigurable RF front-end receiver for cognitive radios.

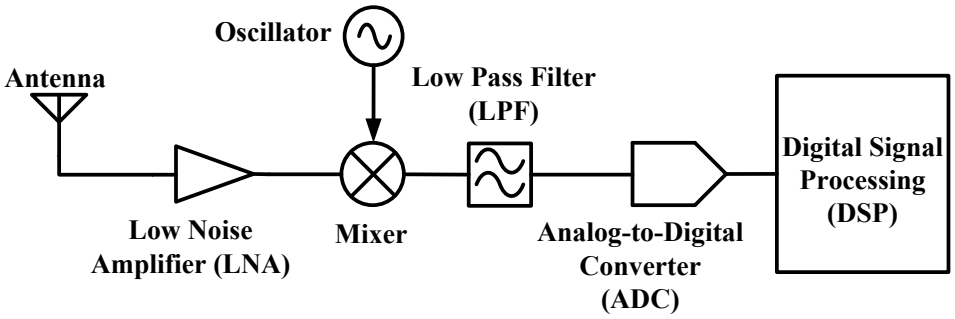

Fig. 46. Basic RF receiver front-end architecture.

In conclusion, a tunable LNA design via a magnetically tunable input matching network is presented. The LNA has been designed and simulated in a 0.13µm CMOS technology and is capable of tuning from 3.2 GHz to 4.6 GHz. The LNA demonstrated a minimum gain of 10 dB and a maximum noise figure of 7.5 dB over the entire tuning range. The core LNA, which excludes the output buffer, consumes 50 mW from a 1.2 V supply.

The author believes the tuning range can be extended with a better phase shifter design capable of provide the necessary phase shift over a wider range of frequencies. The phase shifter is the major limiting factor of tunable LNA design. The phase shifter is capable of providing the necessary phase shift to place the transformer winding currents i_1 and i_2 in phase, as required by magnetic tuning principle. However, the phase shifter only provides it over the frequencies within the LNA's tuning range, a bandwidth of 1.4 GHz. A constant phase shift at all interested frequencies is not achieved, even with a variable resonant tank, the amount of shift decreases at higher frequencies. The design and implementation of a broadband phase shifter capable of constant phase shifts over targeted bandwidths is needed to extend the tuning range of the presented tunable LNA.

Other limitations of the tunable LNA design are noise figure, power and area consumption. The noise figure of the tunable LNA limits the tuning range to avoid reaching undesired high values and signal degradation. The noise figure can be minimized by decreasing the contribution of the major sources of noise, such as the phase shifter. Connecting the phase shifter to the LNA load instead of cascode connection potentially could decrease the overall noise figure of the LNA. Like noise figure, the LNA consumes large amounts of power mainly attributed to the phase shifter. Tradeoffs between bias currents and transistor sizes in the current phase shifter design or a low power phase shifter should be considered to minimize power consumption of the LNA. With the implementation of the transformer and five inductors, three from the phase shifter, the area can be estimated to be quite large. A phase shifter design that minimizes the usage of inductors is needed to reduce the required area of the presented tunable LNA.

BIBLIOGRAPHY

[1] United States Department of Commerce. (2011, Aug.). United States Frequency Allocations Chart 2011. [Online]. Available: http://www.ntia.doc.gov/files/ntia/publications/spectrum_wall_chart_aug2011.pdf

[2] S. Haykins, "Cognitive radio: brain-empowered wireless communications," *IEEE J. Selected Areas in Communications*, vol. 23, pp. 201-220, Feb. 2005.

[3] J. Park et al, "A fully-integrated uhf receiver with multi-resolution spectrum-sensing (MRSS) functionality for IEEE 802.22 cognitive-radio applications," *ISSCC Dig. Tech. papers,* pp. 526-527, Feb. 2008.

[4] B. Razavi, "Challenges in the design of cognitive radios," *IEEE Custom Integrated Circuits Conference*, pp. 391-398, 2009.

[5] A. Bevilacqua and A. M. Niknejad, "An ultrawideband CMOS low-noise amplifier for 3.1-10.6-GHz wireless receiver," *IEEE J. Solid-State Circuits*, vol. 39, pp. 2259-2268, Dec. 2004.

[6] A. Ismail and A. A. Abidi, "A 3-10-GHz low-noise amplifier with wideband LC-ladder matching network," *IEEE J. Solid-State Circuits*, vol. 39, pp. 2269-2277, Dec. 2004.

[7] X. Duo, L. Zheng, M. Ismail, and H. Tenhunen, "Broadband CMOS LNAs for IR-UWB receiver," *NORCHIP Conference*, pp. 273-276, 2005.

[8] D. H. Shin, J. Park, and C. P. Yue, "A low-power, 3 – 5-GHz CMOS UWB LNA using transformer matching technique," *IEEE Asian Solid-State Circuits Conference*, pp. 95-98, 2007.

[9] C. T. Fu and C. N. Kuo, "3 ~ 11-GHz CMOS UWB LNA using dual feedback for broadband matching," *IEEE Radio Frequency Integrated Circuits Symposium*, pp. 67-70, 2006.

[10] M. T. Reiha and J. R. Long, "A 1.2 V reactive-feedback 3.1-10.6 GHz low-noise amplifier in 0.13 μm CMOS," *IEEE J. Solid-State Circuits*, vol. 42, pp. 1023-1033, May 2007.

[11] P. Jamshidi and S. Naseh, "Wideband LNA with reactive feedback at the input matching network," *IEEE Intl. Conference on Electronics, Circuits and Systems*, pp. 330-333, 2011.

[12] Hsien-Ku Chen, Yo-Sheng Lin, and Shey-Shi Lu, "Analysis and design of a 1.6-28-GHz compact wideband LNA in 90-nm CMOS using a π-match input network," *IEEE Trans. Microwave Theory and Techniques*, vol. 58, no. 8, pp. 2092-2104, Aug. 2010.

[13] R. Ramzan, S. Andersson, and J. Dabrowski, "A 1.4 V 25 mW inductorless wideband LNA in 0.13 μm CMOS," *IEEE Intl. Solid State Circuits Conference*, pp. 424-425, 2007.

[14] J. Borremans, P. Wambacq, and D. Linten, "An ESD-protected DC-to-6 GHz 9.7 mW LNA in 90 nm digital CMOS," *IEEE Intl. Solid State Circuits Conference*, pp. 422-423, 2007.

[15] B. G. Perumana, J. H. C. Zhan, S. S. Taylor, and J. Laskar, "A 12 mW, 7.5 GHz bandwidth, inductorless CMOS LNA for low-power, low-cost, multi-standard receivers," *IEEE Radio Frequency Integrated Circuits Symposium*, pp. 57-60, 2007.

[16] G. Sapone and G. Palmisano, "A low-power 3-5-GHz UWB down-converter with resistive-feedback LNA in a 90-nm CMOS process," *European Microwave Integrated Circuits Conference*, pp. 406-409, 2008.

[17] C. W. Kim, M. S. Kang, P. T. Anh, H. T. Kim, and S. G. Lee, "An ultra-wideband CMOS low noise amplifier for 3-5-GHz UWB system," *IEEE J. Solid-State Circuits*, vol. 40, pp. 544-547, Feb. 2005.

[18] C. Huang, C. Chen, and H. Tsao, "A 460MHz~870MHz CMOS wideband low noise amplifier for DVB-T," *IEEE Intl. Symposium on VLSI Design, Automation and Test*, pp. 47-50, 2008.

[19] S. Chehrazi, A. Mirzaei, R. Bagheri, and A. A. Abidi, "A 6.5 GHz wide-band CMOS low noise amplifier for multi-band use," *IEEE Custom Integrated Circuits Conference*, pp. 801-804, 2005.

[20] A. I. A. Galal, R. K. Pokharel, H. Kanaya, and K. Yoshida, "3-7 GHz low power wide-band common gate low noise amplifier in 0.18μm CMOS process," *Asia-Pacific Microwave Conference*, pp. 342-345, 2010.

[21] T. Kihara, T. Matsuoka, and K. Taniguchi, "A 1.0 V, 2.5 mW, transformer noise-canceling UWB CMOS LNA," *IEEE Radio Frequency Integrated Circuits Symposium*, pp. 493-496, 2008.

[22] W. Liou, S. R. Mahendra, and T. Chen, "A wideband LNA design for Ku-band application," *IEEE Intl. Conference on Communications, Circuits and Systems*, pp. 680-684, 2010.

[23] A. Liscidini, C. Ghezzi, E. Depaoli, G. Albasini, I. Bietti, and R. Castello, "Common gate transformer feedback LNA in a high IIP3 current mode RF CMOS front-end," *IEEE Custom Integrated Circuits Conference*, pp. 25-28, 2006.

[24] S. C. Blaakmeer, E. A. M. Klumperink, D. M. W. Leenaerts, B. Nauta, "A wideband noise-canceling CMOS LNA exploiting a transformer," *IEEE Radio Frequency Integrated Circuits Symposium*, 2006.

[25] X. Fan, E. Sánchez-Sinencio, and J. Silva-Martínez, "A 3GHz-10GHz common gate ultrawideband low noise amplifier," *Midwest Symposium on Circuits and Systems*, vol. 1, pp. 631-634, Aug. 2005.

[26] N. Ahsan, A. Ouacha, J. Dabrowski, and C. Samuelsson, “Dual band tunable LNA for flexible RF front end,” *Intl. Bhurban Conference on Applied Sciences and Technology*, pp. 19-22, 2007.

[27] Ying-Che Chung, Chih-Wei Chen, O. T.-C. Chen, and R. Y. J. Tsen, “A multi-band RF front-end receiver for Bluetooth, WCDMA, and GPS applications,” *Midwest Symposium on Circuits and Systems*, vol. 3, pp. 1175-1178, 2003.

[28] A. Savla, A. Ravindran, J. Leonard, and M. Ismail, “System analysis of a multi-standard direct conversion wireless receiver,” Midwest Symposium on Circuits and Systems, vol. 3, pp. 401-403, 2002.

[29] C. Kim, Young-Kyun Jang, and Hyung-Joun Yoo, “Design of CMOS RF front-end for multi-standard receiver (WCDMA and 802.11a),” Intl. Computational Electromagnetics and Its Applications, pp. 340-343, 2004.

[30] S. Yoo and H. Yoo, “Optimazation of switchable inductor and application to reconfigurable LNA with self-matched capacitor,” *Asia-Pacific Microwave Conference*, pp. 1-4, 2007.

[31] V. K. Dao, Q. D. Bui, C. S. Park, "A multi-band 900MHz/1.8GHz/5.2GHz LNA for reconfigurable radio," *IEEE Radio Frequency Integrated Circuits Symposium*, pp. 69-72, 2007.

[32] C. T. Fu, C. L. Ko, C. H. Kuo, and Y. Z. Juang, "A 2.4-5.4-GHz wide tuning-range CMOS reconfigurable low-noise amplifier," *IEEE Trans. Microwave Theory and Techniques*, vol. 56, pp. 2754-2763, Dec. 2008.

[33] M. A. Martins, J. R. Fernandes, M. M. Silva, "Techniques for dual-band LNA design using cascode switching and inductor magnetic coupling," *IEEE Intl. Symposium on Circuits and Systems*, pp. 1449-1452, 2007.

[34] X. Duo, L. Zheng, M. Ismail, and H. Tenhunen, “A concurrent multi-band LNA for multi-standard radios,” *IEEE Intl. Symposium on Circuits and Systems*, vol. 4, pp. 3982-3985, 2005.

[35] H. Hashemi and A. Hajimiri, “Concurrent dual-band CMOS low noise amplifiers and receiver architectures,” *Symposium of VLSI Circuits*, pp. 247-250, 2001.

[36] E. Kargaran and B. Madadi, “Design of a novel dual-band concurrent CMOS LNA with current reuse topology,” *Intl. Conference on Networking and Information Technology*, pp. 386-388, 2010.

[37] Y. C. Chen and C. N. Kuo, "A 6-10-GHz ultra-wideband tunable LNA," *IEEE Intl. Symposium on Circuits and Systems*, pp. 5099-5102, 2005.

[38] Y. Chen, C. Li, J. K. Huang, and C. Kuo, "Low power 3~8-GHz UWB tunable LNA design using SiP technology," *IEEE Intl. Conference on Electronics, Circuits and Systems*, pp. 1026-1029, 2006.

[39] H. Sugawara, Y. Yoshihara, K. Okada, and K. Masu, "Reconfigurable CMOS LNA for software defined radio using variable inductor," *European Conference on Wireless Technology*, pp. 547-550, 2005.

[40] R. J. Weber, *Introduction to Microwave Circuits: Radio Frequency and Design Applications*. Piscataway, NJ: IEEE Press, 2001.

[41] N. M. Neihart, *VLSI Communication Circuits*. Class notes for EE 507, Department of Electrical and Computer Engineering, Iowa State University, Ames, IA, 2009.

[42] B. Razavi, *RF Microelectronics*. Englewood Cliffs, NJ: Prentice Hall, 1998.

[43] D. K. Shaeffer and T. H. Lee, "A 1.5-V, 1.5-GHz CMOS low noise amplifier," *IEEE J. Solid-State Circuits*, vol. 32, no. 5, pp. 745-759, May 1997.

[44] X. Li, "Design of ultra-wideband low noise amplifiers in all-digital 40nm CMOS Technologies," M.S. thesis, Iowa State University, Ames, IA, 2011.

[45] P. Park, C. S. Kim, M. Y. Park, S. D. Kim, and K. K. Yu, "Variable inductance multilayer inductor with MOSFET switch control," *IEEE Electron Device Letters*, vol. 25, pp. 144-146, Mar. 2004.

[46] S. M. Yim and K. O. Kenneth, "Demonstration of a switched resonator concept in a dual-band monolithic CMOS LC-NNED VCO," *IEEE Custom Integrated Circuits Conference*, pp. 205-208, 2001.

[47] H. Sugawara, Y. Yoshihara, H. Ito, K. Okada, K. Masu, "Wide-range RF variable inductor on Si CMOS chip with MEMS actuator," *European Microwave Conference*, pp. 701-704, 2004.

[48] A. Tanabe, K. Hijoka, H. Nagase, and Y. Hayashi, "A novel variable inductor using a bridge circuit and its application to a 5-20 GHz tunable LC-VCO," *J. Solid-State Circuits*, vol. 46, pp. 883-893, Apr. 2011.

[49] Y. S. M. Lee, S. Sheikhaei, S. Mirabbasi, "A 10Gb/s active-inductor structure with peaking control in 90nm CMOS," *IEEE Asian Solid-State Circuits Conference*, pp. 229-232, 2008.

[50] C. H. Wu, J. W. Liao, and S. I. Liu, "A 1 V 4.2mW fully integrated 2.5Gb/s CMOS limiting amplifier using folded active inductors," *IEEE Intl. Symposium on Circuits and Systems*, pp. 1044-1047, 2008.

[51] B. Razavi, "Multi-decade carrier generation for cognitive radios," *Symposium on VLSI Circuits*, pp. 120-121, 2009.

[52] A. Bevilacqua, F. P. Pavan, C. Sandner, A. Gerosa, and A. Nevian, "A 3.4-7 GHz transformer-based dual-mode wideband VCO," *European Solid-State Circuits Conference*, pp. 440-443, 2006.

[53] G. Cusmai, M. Repossi, G. Albasini, A. Mazzanti, and F. Svelto, "A magnetically tuned quadrature oscillator," *IEEE J. Solid-State Circuits*, vol. 42, pp. 2870-2877, Dec. 2007.

[54] J. L. Brown and N. M. Neihart, "An analytical study of a magnetically tuned matching network," *IEEE Intl. Symposium on Circuits and Systems*, pp. , 2012.

[55] M. Soer, E. Klumperink, B. Nauta, and F. van Vliet, "1.5-to-5.0GHz input-matched +2dBm P1dB all-passive switched-capacitor beamforming receiver front-end in 65nm CMOS," *IEEE Intl. Solid-State Circuits Conference Digest of Technical Papers*, pp. 174-176, 2012.

[56] C. Andrews and A. C. Molnar, "Implications of passive mixer transparency for impedance matching and noise figure in passive mixer-first receivers," *IEEE Trans. Circuits and Systems*, vol. 57, no. 12, pp. 3092-3103, Dec. 2010.

[57] X. Tang and K. Mouthaan, "A broadband 180º phase shifter with a small phase error using lumped elements," *Asia Pacific Microwave Conference*, pp. 1315-1318, 2009.

[58] Gyu-Je Sung, "Broadband 90° phase shifter using two short stubs," *IEEE Radio and Wireless Symposium*, pp. 464-467, 2010.

[59] N. Fayyaz, "Variable phase shifter and a system using a variable phase shifter," U. S. Patent 6,906,601, June 14, 2005.

[60] S. Lucyszyn and I.D. Robertson, "Synthesis techniques for high performance octave bandwidth 180° analog phase shifters," *IEEE Trans. Microwave Theory and Techniques*, vol. 40, no. 4, Apr. 1992.

[61] S. Lucyszyn and I.D. Robertson, "Decade bandwidth MMIC analogue phase shifter," *IEE Colloquium on Multi-Octave Microwave Circuits*, pp. 2/1-2/6, 1991.

[62] Y. Zheng and C. E. Saavedra, "An ultra-compact CMOS variable phase shifter for 2.4-GHz ISM applications," *IEEE Trans. Microwave Theory and Techniques*, vol. 56, no. 56, pp. 1349-1354, June 2008.

[63] S.-C. Shin, J.-Y. Huang, K.-Y. Lin, and H. Wang, " A 1.5-9.6 GHz monolithic active quasi-circulator in 0.18 μm CMOS Technology," *IEEE Microwave and Wireless Components Letters*, vol. 18, no. 12, pp. 797-799, Dec. 2008.

[64] S. W. Y. Mung and W. S. Chan, "Novel active quasi-circulator with phase compensation technique," *IEEE Microwave and Wireless Components Letters*, vol. 18, no. 12, pp. 800-802, Dec. 2008.

[65] S. Tanaka, N. Shimomura, and K. Ohtake, "Active circulators-the realization of circulators using transistors," *Proceedings of the IEEE*, vol.53, no. 3, pp. 260-267, March 1965.

[66] H. Hayashi and M. Muraguchi, "An MMIC active phase shifter using a variable resonant circuit," *IEEE Trans. Microwave Theory and Techniques*, vol. 47, no. 10, pp. 2021-2026, Oct. 1999.

[67] D. A. Johns and K. Martin, *Analog Integrated Circuit Design*. Canada: John Wiley & Sons, Inc., 1997.

[68] P. E. Allen and D. R. Holberg, *CMOS Analog Circuit Design Second Edition*. New York, NY: Oxford University Press, 2002.